PALEOCEANOGRAPHY, VOL. 22, XXXXXX, doi:10.1029/2006PA001281, 2007

Ocean circulation at the Last Glacial Maximum: A combined modeling and magnetic proxy-based study

S. J. Watkins,[1] B. A. Maher,[1] and G. R. Bigg[2]

Received 10 February 2006; revised 20 October 2006; accepted 16 November 2006; published XX Month 2007.

[1] Formation of North Atlantic Deep Water (NADW) is an important component of the ocean thermohaline circulation, but debate exists over the ocean circulation state during glacial stages. Some geological and modeling studies suggest decreased NADW and increased formation of Southern Ocean deep water during the Last Glacial Maximum (LGM); others indicate similar, or higher, rates of NADW advection. Here we test three different potential LGM ocean states by comparing the modeled iceberg trajectories each produces with magnetically mapped patterns and sources of LGM ice-rafted debris (IRD). The three LGM states are characterized by vigorous NADW formation; deepwater production in the Southern Ocean; and a third, ''intermediate'' state, with Southern Ocean deepwater formation but also some North Atlantic intermediate water formation. Cluster analysis of sediment magnetic properties was used to characterize North Atlantic IRD patterns and sources, which match most closely iceberg trajectories arising from some combination of the ''southern sinking'' and ''intermediate'' ocean circulation states. The magnetic data indicate two major IRD sources, Fennoscandia and Greenland/Iceland, and one minor source, the St. Lawrence region. The model and magnetic data suggest that the LGM North Atlantic circulation was dominated by a cyclonic central North Atlantic gyre, separated from the North Atlantic Current, which was displaced south of ~42N.

Citation: Watkins, S. J., B. A. Maher, and G. R. Bigg (2007), Ocean circulation at the Last Glacial Maximum: A combined modeling and magnetic proxy-based study, *Paleoceanography*, *22*, XXXXXX, doi:10.1029/2006PA001281.

1. Introduction

[2] Understanding the circulation of the North Atlantic is crucial given the key role the ocean plays in controlling the global oceanic and atmospheric circulation through the thermohaline circulation (THC) and the transfer of heat from the equator to the poles. Evidence, both from ocean general circulation models and marine sediment studies, suggests the strength of the THC may have varied through time and possibly undergone complete shutdown, altering global ocean circulation (see, e.g., review of *Rahmstorf* [2002] or *Seidov et al.* [2001]). Much debate currently exists over the circulation of the North Atlantic during the Last Glacial Maximum (LGM). Three conflicting theories have emerged from both modeling and geological proxy-based studies. The first theory suggests there was very little or no production of deep water in the North Atlantic, with much greater influence and penetration of deep water formed in the Southern Ocean [e.g., *Oppo and Fairbanks*, 1987; *Michel et al.*, 1995; *Kim et al.*, 2003; *Keigwin*, 2004; *Robinson et al.*, 2005]. The second circulation state identifies production at the LGM of North Atlantic Deep Water (NADW) at a similar location and with similar (or possibly stronger) formation rates to the present day [e.g., *Yu et al.*, 1996; *Hewitt et al.*, 2003]. The third state is characterized by production of intermediate depth water (with a more limited distribution) in the North Atlantic, while the deep ocean basins are dominated by water formed in the Southern Ocean [e.g., *Boyle and Keigwin*, 1987; *Sarnthein et al.*, 1994, 1995; *Beveridge et al.*, 1995; *Seidov and Haupt*, 1997; *Ganopolski et al.*, 1998; *Shin et al.*, 2003]. The location of formation of intermediate depth water is debated, but is suggested to have shifted southward to ~50–60N [e.g., *Duplessy et al.*, 1980; *Sarnthein et al.*, 1995; *Seidov et al.*, 1996; *Seidov and Haupt*, 1997]. The strength of this intermediate water formation is also unclear; proxy data reconstructions and modeling studies suggest anything from very little reduction to a 50% reduction compared to the present day [*LeGrand and Wunsch*, 1995; *Seidov et al.*, 1996; *Seidov and Haupt*, 1997; *Marchal et al.*, 2000; *Schäfer-Neth and Paul*, 2000; *McManus et al.*, 2004].

[3] One way of testing these three circulation states is through identification of the spatial distribution of iceberg-rafted debris (IRD) in the North Atlantic, the bergs having been transported by dominant surface water currents during the LGM. So far, while there have been studies of IRD associated with past glacial stages [e.g., *Ruddiman*, 1977; *Fillon et al.*, 1981; *Smythe et al.*, 1985; *Balsam and McCoy*, 1987; *Cremer et al.*, 1992], relatively few studies of Atlantic-wide IRD patterns have been reported for the LGM. The most complete study to date of LGM IRD in the North Atlantic is provided by *Robinson et al.* [1995], who identified differences between sediment magnetic susceptibility values at the LGM and in the Holocene, in order to identify regions of increased ice rafting.

[1]Centre for Environmental Magnetism and Palaeomagnetism, Lancaster Environment Centre, Geography Department, Lancaster University, Lancaster, UK.

[2]Department of Geography, University of Sheffield, Sheffield, UK.

0883-8305/07/2006PA001281$12.00

Table 1. Contrasting Characteristics of the Ocean Circulation for the Three Model States[a]

	NSS	SSS	ISS
Thermohaline circulation	Vigorous formation of NADW (56 Sv), very little southern-sourced deep water	deep water produced in Southern Ocean (12 Sv), very weak production of North Atlantic intermediate water (2 Sv)	formation of intermediate water in North Atlantic (10 Sv) and deep water in Southern Ocean
East Greenland Current	Southward flowing EGC, northward extension of NAC	southward extension of EGC	no southward EGC north of ~65N; southward extension of EGC south of ~60N
North Atlantic Current	Strong, easterly NAC	weaker, more zonal NAC	Weaker, more zonal NAC
Flow at European coast	northeasterly flow along European coast	northeasterly flow along European coast	Flow toward European coast

[a]Abbreviations are NADW, North Atlantic Deep Water; EGC, East Greenland Current; and NAC, North Atlantic Current.

[4] Here we extend *Robinson et al.*'s [1995] study, by using two different approaches to identify iceberg trajectories and IRD, and hence dominant ocean circulation, patterns. First, we use iceberg trajectory modeling within three different modeled LGM ocean circulation states, in order to identify the links between surface currents and possible loci of deep water formation. Second, to reconstruct ocean surface currents, we use a suite of magnetic measurements to characterize magnetically IRD in LGM sediments from deep-sea cores spread across the North Atlantic and neighboring seas, comparing the sediment magnetic signatures with a range of circum-Atlantic potential sediment source materials [*Watkins and Maher*, 2003]. On the basis that iceberg drift and melting reflect ocean surface currents across the North Atlantic at the LGM, and that we can identify magnetically the distributions and generalized sources of LGM IRD, we can compare the modeled and our inferred IRD patterns to thence enable identification of the most probable LGM ocean circulation state.

2. Methods

2.1. Iceberg Modeling

[5] In the modeling approach, an iceberg model is used to investigate the effect of surface circulation patterns on iceberg drift, a model previously validated in reproductions of present-day iceberg distributions in both the Arctic [*Bigg et al.*, 1996] and Antarctic [*Gladstone et al.*, 2001]. Brief details are given below (a fuller discussion is given by *Bigg et al.*, 1996, 1997; *Gladstone*, 2001 and *Gladstone et al.*, 2001]. The model, including both dynamical and thermodynamical processes, is driven by gridded atmospheric (temperature and wind) and oceanic (temperature, surface current and sea ice) forcing fields and aims to reproduce the main features of iceberg trajectories in the North Atlantic, although it is well known that ocean currents provide the dominant forcing for iceberg trajectories [e.g., *Smith and Banke*, 1983; *Bigg et al.*, 1997]. A number of melting processes are parameterized: wave erosion, basal melting and sidewall convection, solar and sensible heating, and sublimation. Most of these processes increase with water temperature, but wave erosion becomes dominant away from polar regions [*Bigg et al.*, 1997]. The model is initialized with icebergs of different sizes released from a number of circum–North Atlantic sources. Iceberg sizes and release sites depend on the calving flux, here estimated from a mass balance analysis of LGM northern hemisphere ice sheets [*Bigg and Wadley*, 2001]. In total, 419 icebergs are released from 61 different sites. The total iceberg flux is then scaled up by relating the calculated annual mass flux from each release site [*Bigg and Wadley*, 2001] to the flux deriving from the limited suite of icebergs released at each site. At the end of each time step, the new position, velocity, dimensions and mass of each iceberg are calculated. If an iceberg collides with the coastline, it is removed from the model. If, near the coast, the iceberg moves into an area where the water is shallower than its draft, it becomes grounded and continues to melt until it can refloat and move away.

[6] Annual mean forcing fields from an atmospheric general circulation model (AGCM) and ocean general circulation model (OGCM) are used to drive the iceberg model. Here three LGM circulation states, with very different circulation characteristics aiming to represent to some degree the three different North Atlantic paleoceanographic views of LGM circulation discussed above, were obtained using two modeling approaches. The main features of these three circulation states are shown in Table 1. In the first approach, LGM AGCM fields from *Hall et al.* [1996] are used to drive indirectly an OGCM [*Bigg et al.*, 1998]. The resulting oceanic forcing fields (4 longitude by 3 latitude resolution and 19 vertical levels) are then used as relaxation constraints in a robust mode model to produce finer resolution (1 $\times$ 1 and 19 vertical levels) fields for use with the iceberg model. Global sea levels at the LGM were ~120 m lower than present day [*Fairbanks*, 1989]; thus an LGM coastline was determined from the *Peltier* [1994] ice sheet topography. Topography is taken from the *ETOPO* [1986] $5' \times 5'$ depth and elevation data set. This OGCM was forced into two differing, stable LGM circulation states. The model naturally falls into a first state, the "northern sinking state" (NSS), with strong North Atlantic overturning. The second state, the "southern sinking state" (SSS) with little convection in the North Atlantic, is obtained by adding a freshwater anomaly of 1 mm d^{-1} over the North Atlantic, N of 42N, for 500 years.

[7] A third state, the "intermediate sinking state" (ISS) is produced using a different OGCM [*Wadley and Bigg*, 2002; *Wadley et al.*, 2002]. Instead of a regular latitude-longitude grid, the model uses a curvilinear grid, with the model grid's North Pole in Greenland. This gives a coarse resolution in the far field but in the northern Atlantic the resolution is roughly 1–2. Thus the modeled forcing fields were interpolated back to a regular latitude-longitude grid (1 $\times$ 1) for use in the iceberg model. The LGM simulation was produced by adjusting the present-day fluxes with LGM minus present-day difference fields of wind stress, freshwater flux and

surface air temperature (from the AGCM of *Dong and Valdes* [1998]), with an additional freshwater flux of 1 mm d^{-1}, added between 60 and 75N. This was done to produce an ocean circulation, particularly in the Atlantic, most compatible with proxy records of sea surface temperature, oxygen isotopic records and intermediate depth sinking pathways for "deep" water formed in the northern Atlantic. Thus, in this state, North Atlantic convection occurs to intermediate depths in the central west North Atlantic, around 50–60N.

[8] This third state is the one that would be expected to be, a priori, the best representation of the LGM ocean. The NSS state illustrates a case of an extreme overturning, perhaps compatible with the short periods of sudden warmings experienced during glacial periods, while the SSS state illustrates the response of the ocean to a major and sustained freshwater input to the North Atlantic. While none of the three states will correspond precisely to any real glacial ocean state, particularly as these runs do not have an active sea ice model, they cover the range of likely circulations seen in the ocean during a glacial period. One can, also, ask whether the 1 resolution ocean fields used to force the iceberg trajectory model are sufficiently detailed to produce realistic trajectories, particularly in view of the importance of coastal boundary currents in advecting bergs away from calving sites. Despite the limitations in ocean representation, such resolution has been shown to be sufficient in present-day simulations for the North Atlantic to reproduce realistic geographic envelopes of iceberg trajectories [*Bigg et al.*, 1996]. The pattern differences, if not the detail, in iceberg trajectories between the three ocean states should therefore be robust. It is also worth remembering that knowledge of the LGM ocean circulation can never be better than the imprecise estimate of the atmospheric forcing produced by much coarser atmospheric circulation models.

2.2. Sediment Proxy Data

[9] To determine LGM iceberg distributions, magnetic susceptibility and a suite of room temperature remanences were used to characterize and trace IRD in deep-sea sediments right across the North Atlantic. In total, 154 North Atlantic deep-sea sediment samples were obtained, from cores with existing chronologies based on δ^{18}O records and ^{14}C dating. All the sampled core sections fall within the LGM interval of 18–24 cal kyr B.P. and the sample lying centrally within the LGM interval of stable δ^{18}O values was used in each case (see auxiliary material).[1] The magnetic methods used follow those used to characterize modern day North Atlantic sediments and sources [*Watkins and Maher*, 2003]; details are given in the auxiliary material. The magnetic signature of a sample reflects its magnetic mineralogy and magnetic grain size. (Magnetic grain size should not be confused with clastic particle size; for example, large clastic particles might contain fine, magnetically single domain magnetic grains - ~0.05 μm in magnetite). We previously measured the magnetic properties of a number of potential source samples all around the North Atlantic, to make detailed comparison with the magnetic "fingerprints" of both our LGM and present-day sediment samples, in order to constrain their sources where robustly possible [*Watkins and Maher*, 2003]. Samples from potential sediment source areas were collected from: north African soils; European and American loess; Icelandic basalts and volcanic ash; Devonian and Triassic red beds from Spitsbergen and East Greenland, respectively; Caribbean carbonates containing bacterial magnetite; granites from north Bylot Island; and a range of other lithologies from the circum-Atlantic area (see section 3.2 and *Watkins and Maher* [2003]). Present-day regions of high iceberg flux and melting are strongly associated with distinctive source and sediment magnetic properties [*Watkins and Maher*, 2003], often characterized by the presence of strongly magnetic, magnetically coarse-grained, detrital components. Strongly magnetic material, e.g., originating from the Mid-Atlantic Ridge, may also be transported and/or scoured by bottom water currents, e.g., in the South Iceland Basin by Iceland-Scotland Overflow water [e.g., *Kissel et al.*, 1999]. However, statistically significant changes in sediment magnetic mineralogy along the path of deep water currents suggest that other detrital inputs additionally contribute within these linear depositional zones at the present day [*Watkins and Maher*, 2003]. Other deep sea processes may also lead to differential settling and/or removal of fine-grained IRD.

[10] A suite of susceptibility and remanence measurements was applied to all samples with the aim of characterizing their magnetic mineralogy, concentration and magnetic grain size (domain state). Prior to measurement, wet samples were dried at 40C, gently disaggregated and packed into plastic sample holders, with sample weights measured to allow for correction of magnetic measurements to a dry mass-specific basis. We use the sediment magnetic properties as a tracer, or "fingerprint," not as an indicator of either magnetic concentration or sediment volume. Indeed, in order to remove variations caused by changes in magnetic concentration (because of possible biogenic dilution and/or variations in sedimentation rates), interparametric ratios were calculated from the susceptibility values (measured at low and high frequencies) and the anhysteretic and remanent magnetizations [see, e.g., *Maher et al.*, 1999] for a summary of magnetic parameters and their application to environmental contexts). Geographic plots of the data were generated using ArcMap, each sample point being represented by a shaded area of 5 radius.

[11] To identify independently the presence of coarse clastic particles (>150 μm), i.e., unambiguously diagnostic of IRD origin, within our deep sea samples, we applied sediment dispersion and wet sieving to a representative geographic subset, comprising 46 samples (24 pelagic and 22 hemipelagic sites). While such coarse particles might be diagnostic of IRD origin [e.g., *Andrews et al.*, 1998; *Bond et al.*, 1997], most IRD is composed of particles <150 μm [e.g., *Prins et al.*, 2002; *Farmer et al.*, 2003]. Hence, to characterize the sediments robustly, magnetic measurements were made of bulk samples, not the coarse-grained fractions.

[12] Given the reasonably large, multiparameter magnetic data set produced from the sediment samples, two multivariate methods were used to analyze the data subsequently,

[1]Auxiliary material data sets are available at ftp://ftp.agu.org/apend/pa/2006pa001281. Other auxiliary material files are in the HTML.

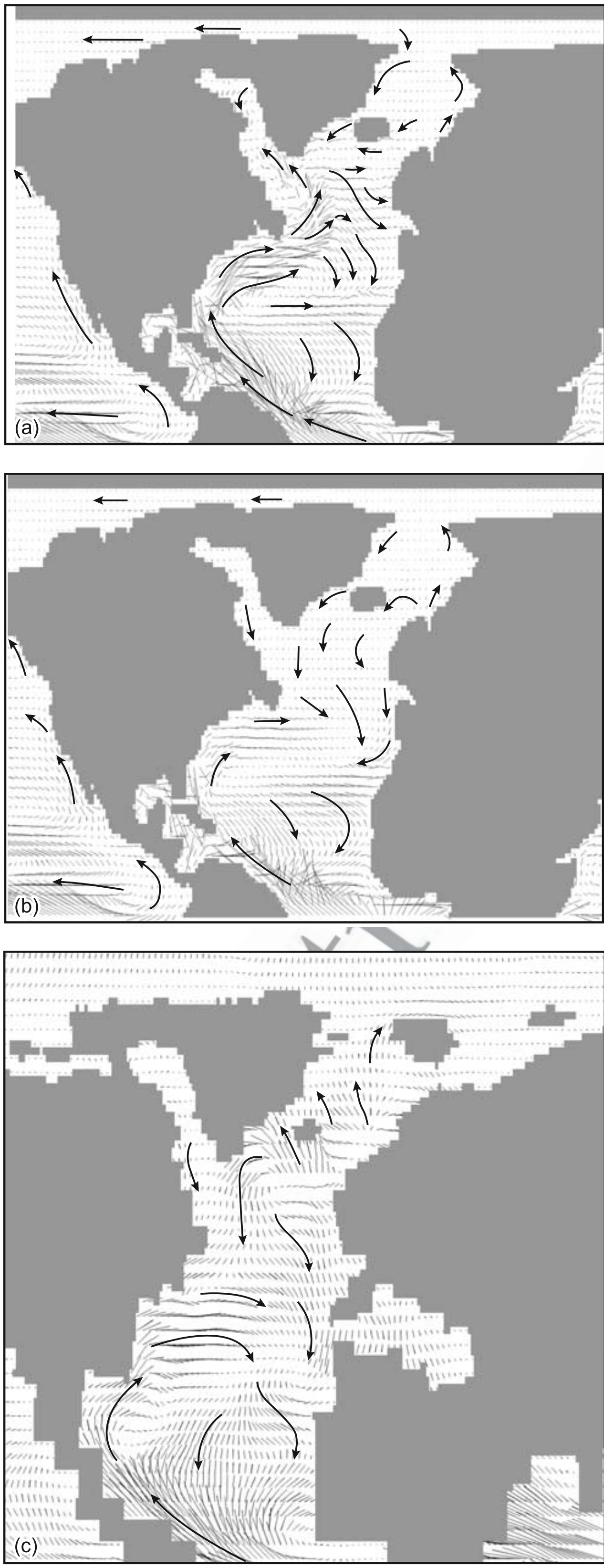

Figure 1. Predicted surface currents for the three modeled LGM circulation states: (a) NSS, (b) SSS, and (c) ISS. Note that the ISS results are derived from a different atmosphere-ocean general circulation model (AOGCM) based on a curvilinear (rather than regular latitude-longitude) grid; see section 2.1. In this case, note that the surface wind-driven current shown here, and affecting the icebergs, does not show the subsurface northeastward current in the central Atlantic supplying the model's convection site southeast of Greenland.

in order to try to discriminate between possible sediment groupings and therefore sources, and also identify any mixing between sources. Fuzzy c means clustering and nonlinear mapping, using the program of *Vriend et al.* [1988], were used, so that samples are not forced to belong to an individual cluster; instead, their degree of affinity with each identified cluster is calculated. Fuzzy clustering was run using four, independent, nonconcentration-dependent magnetic parameters in order to differentiate sediments based on the magnetic "signatures" of their constituent magnetic grains: (1) the high field remanence (the HIRM, as a percentage of the saturation remanence, SIRM), to identify the presence of high-coercivity minerals, such as haematite and goethite; (2) frequency-dependent magnetic susceptibility (χ_{fd}), to identify, where present, ultrafine-grained ($<\sim$20 nm), superparamagnetic (SP) ferrimagnets (such as magnetite and maghemite), often of soil-formed origin [e.g., *Maher*, 1998]; (3) the ratio of the anhysteretic remanence normalized to magnetic susceptibility (χ_{ARM}/χ_{lf}), to identify fine-grained ($\sim$30–50 nm), single domain (SD) ferrimagnets, and (4) the "soft" remanence fraction, i.e., that acquired at the relatively low magnetic field of 20 mT (the IRM_{20mT}/IRM_{100mT}), to identify low-coercivity, coarse-grained (multidomain, MD-like) ferrimagnets. The magnetic parameters were investigated using the nonparametric Spearman's test to ensure they were not autocorrelated. Four samples were identified as outliers (i.e., values more than 3 times the standard deviation from the mean) and removed from the data set to preclude undue influence on the clustering, leading to unrealistic groupings [*Hanesch et al.*, 2001]. Finally, values were standardized so that parameters with large values and/or variability again did not predominate.

3. Results

3.1. Iceberg Model

[13] The modeled surface currents and iceberg trajectories arising from each of the three ocean circulation states are shown in Figures 1 and 2. Five key regions where the modeled iceberg trajectories differ between the three circulation states are identified below and summarized in Table 2.

3.1.1. South of Greenland

[14] In both the SSS and ISS states, icebergs are transported in a net sense southward from Greenland; any IRD in these icebergs would thus be dominated by ferrimagnets from igneous provinces. In contrast, in the NSS model, icebergs from Greenland are blocked from southward travel because of the more northerly position of the North Atlantic Current (NAC). Instead, NSS icebergs are transported

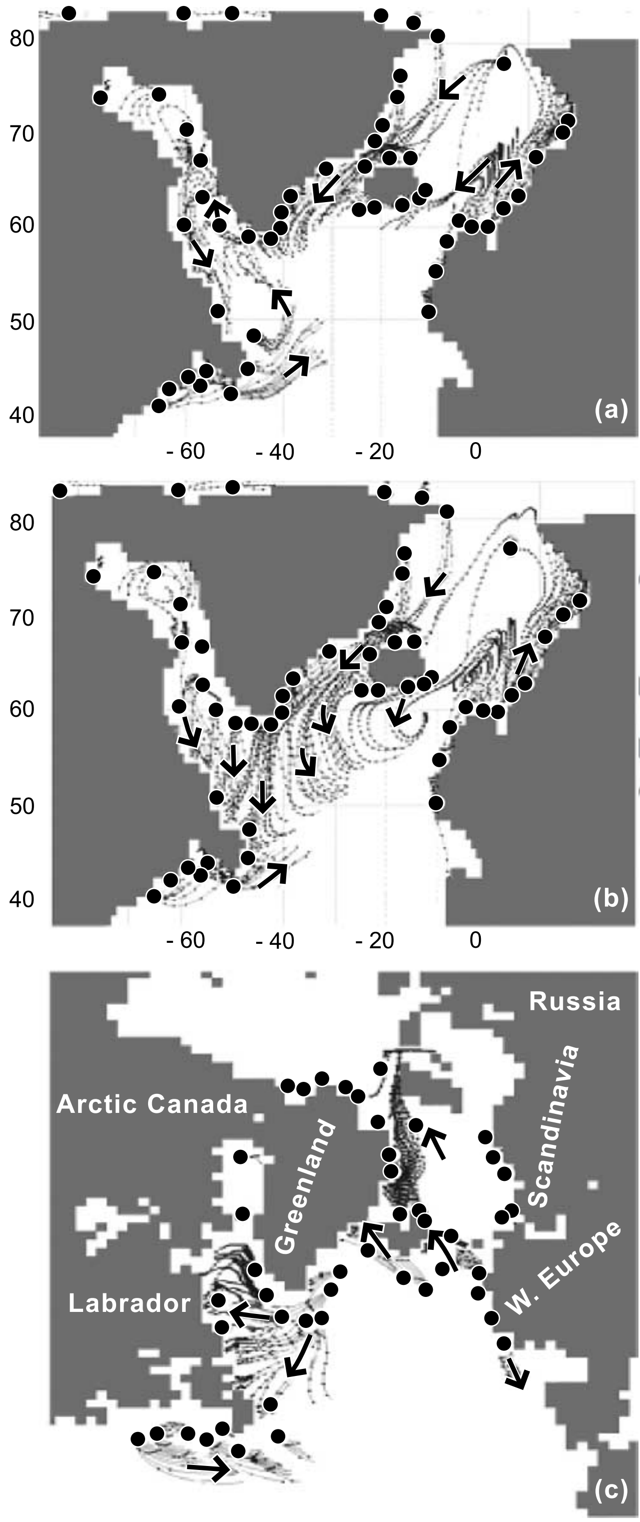

Figure 2. Predicted iceberg trajectories for the three modeled LGM circulation states: (a) NSS, (b) SSS, and (c) ISS. As with Figure 1, note that the ISS results are derived from a different AOGCM based on a curvilinear (rather than regular latitude-longitude) grid; see section 2.1.

northward from the St. Lawrence. Any IRD from this region would be likely to contain a significant amount of high-coercivity minerals from red sandstones present in the St. Lawrence region. Note that in all cases, bergs from SE Greenland travel southward, while those from SW Greenland are entrained within the Labrador Sea gyre.

3.1.2. Labrador Sea

[15] In the NSS simulation, none of the icebergs released from S and SW Greenland survive long enough to be transported into the Atlantic; they melt in the warmer waters associated with the northerly branch of the NAC. In contrast, icebergs in the SSS and ISS simulations are transported generally around the Labrador Sea and so then southward but do not enter the North Atlantic, eventually grounding along the Labrador coast.

3.1.3. East Greenland

[16] While the NSS and SSS simulations are both characterized by southward transport of icebergs along the East Greenland coast in an East Greenland Current, the ISS simulation is very different. There is very little iceberg activity between $\sim$65 and 70N in the ISS because of the presence of strong onshore currents. Icebergs in the SSS and ISS models travel significantly further south ($\sim$7) than in the NSS, reflecting the colder sea surface temperatures of these two states, particularly the SSS.

3.1.4. St. Lawrence

[17] The majority of icebergs released from the St. Lawrence region are transported eastward, although in the NSS, those released to the east of Newfoundland are transported northward. Maximum easterly iceberg extents are 30W in the NSS, 35W in the SSS and 40W in the ISS. However, very few icebergs actually reach these maximum extents. Plots of the iceberg contribution to meltwater indicate that the majority of these icebergs melt close to the release sites.

3.1.5. South of Iceland

[18] Close to the western coast of Europe, the NSS and SSS iceberg trajectories are similar, with a large number of icebergs melting close to the iceberg release sites. Some European icebergs are transported westward and become entrained in a cyclonic gyre, which transports the icebergs southward toward Iceland. These icebergs are transported $\sim$5 farther south in the SSS simulation and mix with icebergs released from southern Iceland. In contrast, the ISS is dominated by two areas of divergence, which create coastward flowing currents causing most of the European icebergs to collide with the coast immediately after release.

3.2. Magnetic Measurements

[19] Magnetic susceptibility (χ_{lf}) provides an indication of how magnetic a sample is, often reflecting its concentration of ferrimagnets [e.g., *Thompson and Oldfield*, 1986]. Magnetic susceptibility values for the LGM North Atlantic sediments range from 0.01 to 6.6 $\times$ 10^{-6} m^3 kg^{-1} (Figure 3). The data identify a major contrast between the lowest values (<0.5 $\times$ 10^{-6} m^3 kg^{-1}) at low latitudes (south of $\sim$40N) and higher and more variable values at middle to high latitudes. This pattern persists even when adjustment of the susceptibility data is made for carbonate content (Figure 4), indicating that changes in detrital magnetic input are more significant for the sediment magnetic properties

Table 2. Summary of the Main Regions of Differences in Iceberg Trajectories (and Thus Meltwater) Between the Three LGM Circulation States

Region	NSS	SSS	ISS
South of Greenland	northward flow of St. Lawrence icebergs, Greenland icebergs melted by ~57N	southward flow of Greenland icebergs to ~40 to 45N	southward flow of Greenland icebergs to ~45N
Labrador Sea	gyre-like circulation, similar to present day	only southward transport of icebergs	south and SW transport of icebergs
St. Lawrence	easterly extent ~30W	easterly extent ~35W	easterly extent ~40W
South of Iceland	some European icebergs, southerly extent ~60N	European and Icelandic icebergs, southerly extent ~55N	very little iceberg activity
East Greenland	southerly EGC, limited iceberg trajectories, easterly extent ~35W, southerly extent ~57N	southerly EGC, widespread iceberg trajectories, easterly extent ~25W, southerly extent ~50N	northerly EGC north of 70N, coastward flow between 65 and 70N, southward flow south of 65N but only close to coast

than the diamagnetic (diluting) effects of carbonate content. The low susceptibility values observed at low latitude, pelagic sites are similar to those of our measured African soil samples (Figure 3) [*Watkins and Maher*, 2003] and suggest aeolian transport and sedimentation at these latitudes. Conversely, higher susceptibility values (0.5–6 × 10^{-6} m^3 kg^{-1}) occur mainly in the northern North Atlantic (to ~50N) but also extend to pelagic sediments as far south as ~32N. Also shown on Figure 3 (and Figure 4) are the approximate pathways of North Atlantic deep water [from *Kissel et al.*, 1999]. The LGM high susceptibility zone extends well beyond these linear trajectories of bottom water transport. The higher susceptibility values are similar to those obtained for potential source samples of igneous (e.g., Icelandic basalt and north Bylot Island granite) rocks (Figure 3), and given their extremely wide spatial distribution across the floor of the North Atlantic Ocean, most likely reflect input of IRD from these and/or similar igneous provinces [e.g., *Linthout et al.*, 2000]. A geographic subset of our LGM samples (the starred points in Figure 3) were sieved and all found to contain rock particles >150 μm, i.e., particles unambiguously of IRD origin (see auxiliary material). In spatially restricted areas of the North Atlantic (such as more proximal, hemipelagic sites or linear zones affected by bottom water transport), it is possible that strongly magnetic IRD might have been subjected to some post-LGM redistribution by turbidite or bottom water transport, or that part of the magnetic signature is contributed by sediment sources other than IRD. For instance, at the present-day, sediments deposited by deep water currents along the eastern Mid-Atlantic Ridge, south of Iceland, are magnetically similar to other, strongly magnetic sediments offshore from iceberg-calving sites [*Watkins and Maher*, 2003]. However, even where non-IRD sources have previously been thought to be dominant (e.g., the Iceland-Scotland channel, the Irminger Basin [*Kissel et al.*, 1997,

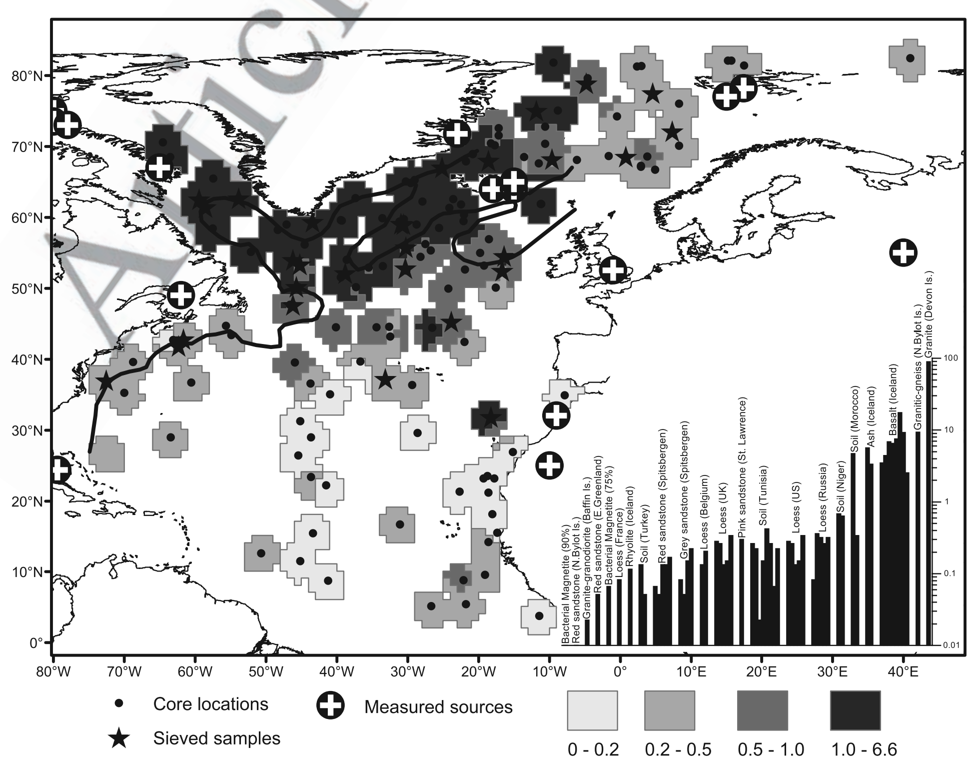

Figure 3. Magnetic susceptibility values (×10^{-6} m^3 kg^{-1}) in LGM North Atlantic deep-sea sediments and a range of potential source samples.

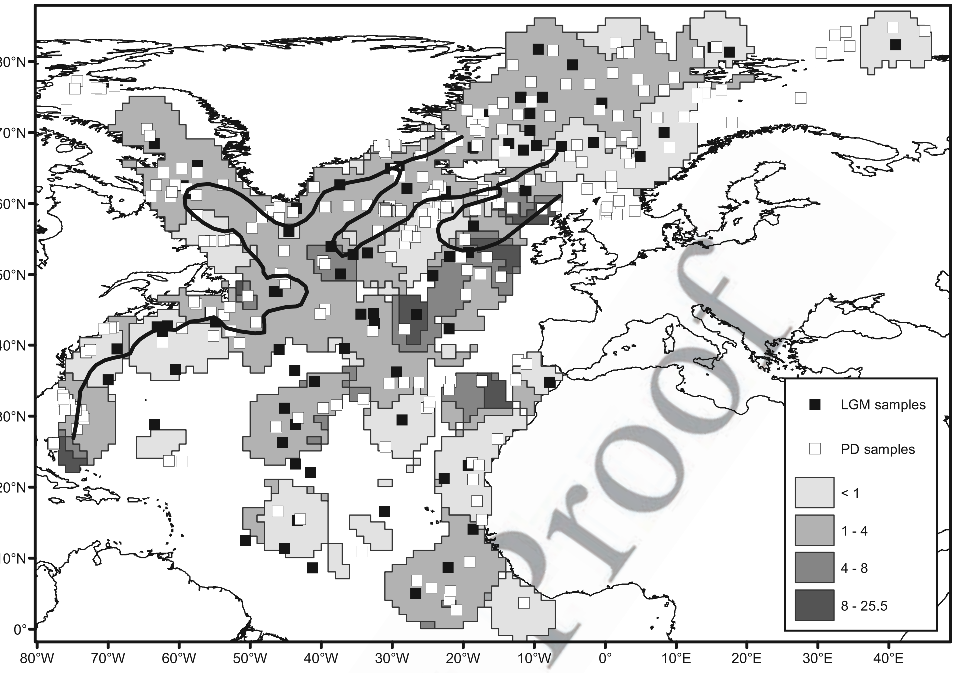

Figure 4. Calcium carbonate values (%) in LGM North Atlantic deep-sea sediments, with additional data from *Balsam and McCoy* [1987], *Kassens* [1990], *Hillaire-Marcel et al.* [1994], *Stein et al.* [1995], *Vogt* [1997], *Knies* [1999], *de Vernal and Hillaire-Marcel* [2000], J. Andrews, personal communication, 2003, and M. Pirrung, personal communication, 2003.

1999; *Kissel*, 2005]), recent studies have identified the additional and significant presence of IRD [e.g., *St. John et al.*, 2004; *Prins et al.*, 2002]. Further, bottom current intensity is thought to have decreased during periods of enhanced iceberg discharge [*Kissel*, 2005].

[20] Figure 5 shows the difference in sediment magnetic susceptibility at the LGM compared with the present day. For the majority of the North Atlantic floor, significantly more magnetic (i.e., up to $\sim$20 $\times$ more magnetic) deep-sea sediment was deposited at the LGM. Major zones of magnetic susceptibility increases occur to the NW and SW of the U.K., SE of Greenland, and NW of the African coast.

[21] Frequency-dependent susceptibility (χ_{fd}) values in the LGM North Atlantic range from 0.5–14% (Figure 6) and display an almost inverse relationship to susceptibility. Highest values (6–14%) are located at low latitudes (south of

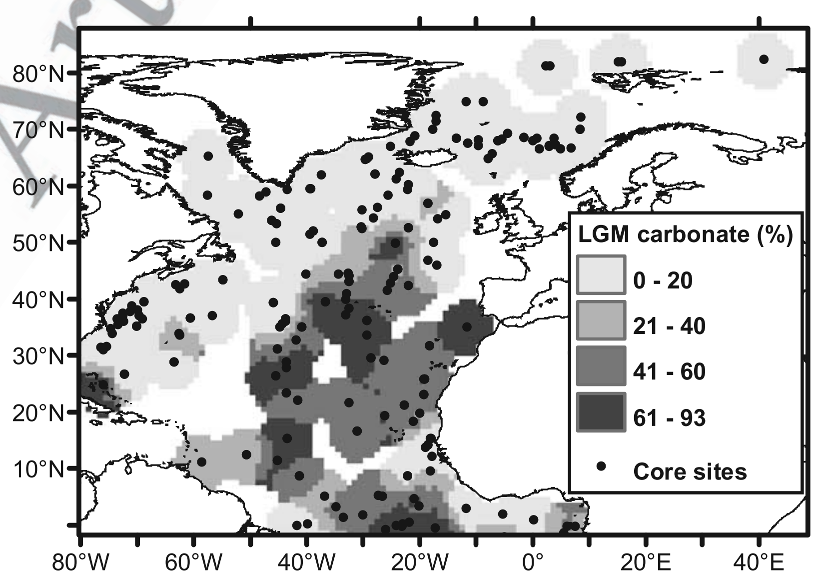

Figure 5. Ratio of magnetic susceptibility ($\times 10^{-6}$ m^3 kg^{-1}) at the LGM compared to the present day (PD). Ratios were calculated by interpolating LGM and PD values to a 1 $\times$ 1 grid. Values >1 identify enhanced magnetic concentrations at the LGM.

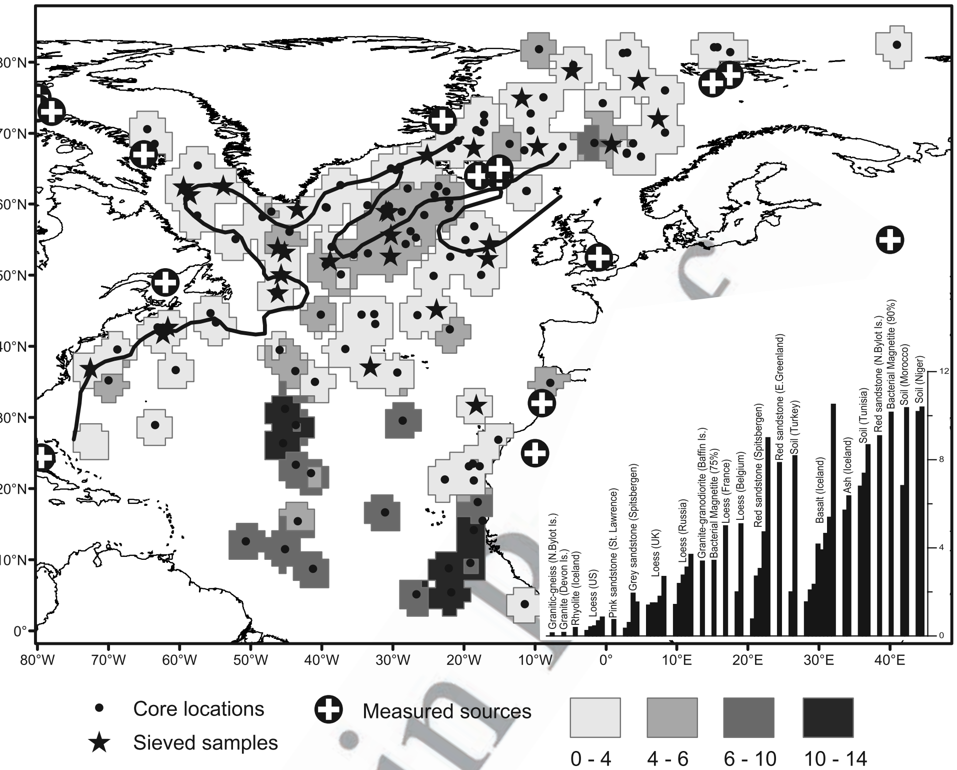

Figure 6. Frequency-dependent magnetic susceptibility values (%) in LGM North Atlantic deep-sea sediments and a range of potential source samples.

~30N) in a region extending west (to ~50W) from Africa. Values as high as 14%, which indicate the dominance of ultrafine-grained, superparamagnetic (SP) ferrimagnets [*Maher*, 1988; *Dearing et al.*, 1996], are also displayed by our measured African soil samples (Figure 6). Values of frequency-dependent susceptibility at middle to high latitudes are mostly <4%; our measured igneous rocks (granitic rocks from Baffin, Devon and north Bylot Islands) have similarly low χ_{fd} values. The region south of Iceland is characterized by intermediate χ_{fd} values (4–6%) and high χ_{lf} values, similar to modern samples of Icelandic ash.

[22] High field remanence (the remanence acquired in fields between 0.3 and 1 T, as a percentage of the total remanence) can be used to investigate the presence of weakly magnetic, high-coercivity minerals, such as haematite and goethite. HIRM values in the LGM North Atlantic range from 0.3–38% (Figure 7), with two particular regions of high values (>10%). The first of these, found to the west of Africa (south of ~25N), coincides with low χ_{lf} and high χ_{fd} values, again substantiating the aeolian transport and deposition of haematite- and goethite-rich North African soils [*Robinson*, 1986; *Maher and Dennis*, 2001] (Figure 7). In contrast, the second region of high values (east of the North American coast, between 20 and 50N) is associated with low χ_{lf} and χ_{fd} values. While it is possible that this region might have experienced some distal African dust input [e.g., *Prospero et al.*, 1981; *Balsam et al.*, 1995], these magnetic data instead suggest these sediments contain coarser-grained, and therefore possibly originally glacially derived, red bed material from the St. Lawrence region. Red bed source samples from the St. Lawrence lowlands have the highest HIRM values (>50%) of any of our potential source samples (Figure 7). Smaller regions of intermediate HIRM values west of the UK and in the eastern Nordic Seas may similarly indicate the transport of haematite-derived IRD, from Precambrian, Carboniferous and Devonian sandstones of NW Scotland, England and Wales, and Spitsbergen. Lowest HIRM values, similar to those of the measured igneous source rocks (Icelandic basalts and rhyolites, Devon Island granite and north Bylot Island granitic-gneiss, Figure 7) are located around Iceland, around Greenland, and throughout the Labrador Sea.

[23] The proportion of remanence acquired at low applied fields (here the IRM acquired at 20 mT, normalized to the remanence acquired at 100 mT) can be used as an indicator of ferrimagnetic grain size (domain state). High values of this parameter indicate higher concentrations of ferrimagnets that are easy to magnetize, i.e., either coarse multidomain grains or fine, magnetically viscous grains on the single domain/superparamagnetic border [e.g., *Maher et al.*, 1999]. Values for the LGM deep-sea sediments range from 0.01 to 0.6 (Figure 8). The highest ratios are located in the low χ_{lf}, and high χ_{fd} and HIRM region to the west of Africa, and reflect the presence of the fine and ultrafine, viscous single domain/superparamagnetic grains in soil-derived dust (Figure 8). In contrast, the area to the east of the North American coast is characterized by the lowest values (<0.15), most likely reflecting the presence of

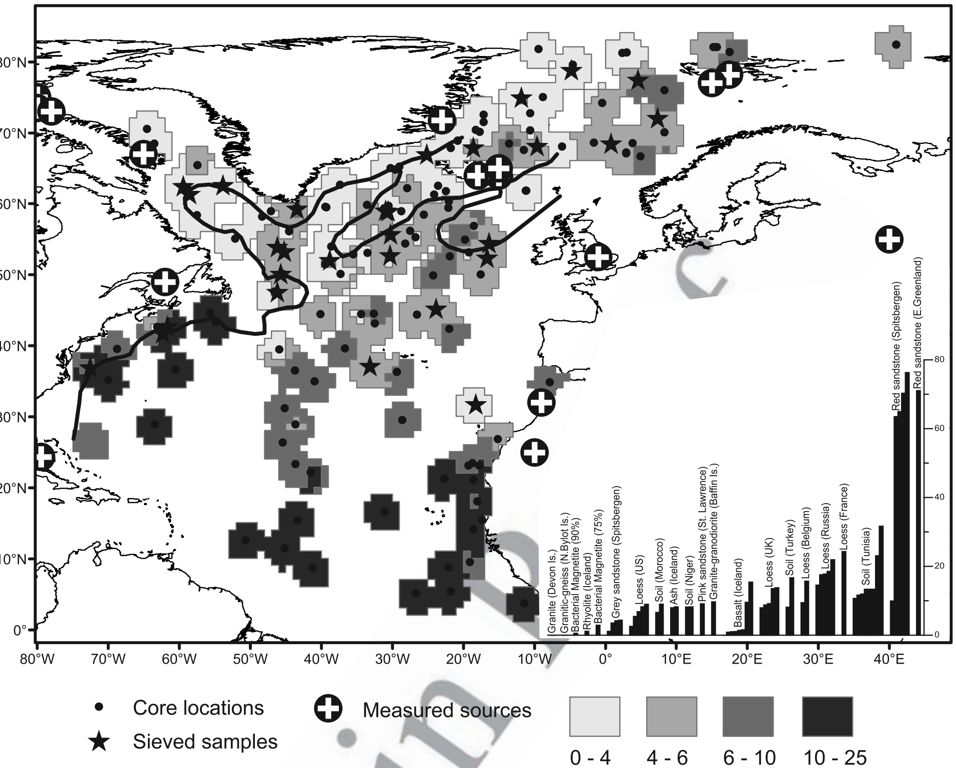

Figure 7. High field remanence (HIRM) values (%) in LGM North Atlantic deep-sea sediments and a range of potential source samples.

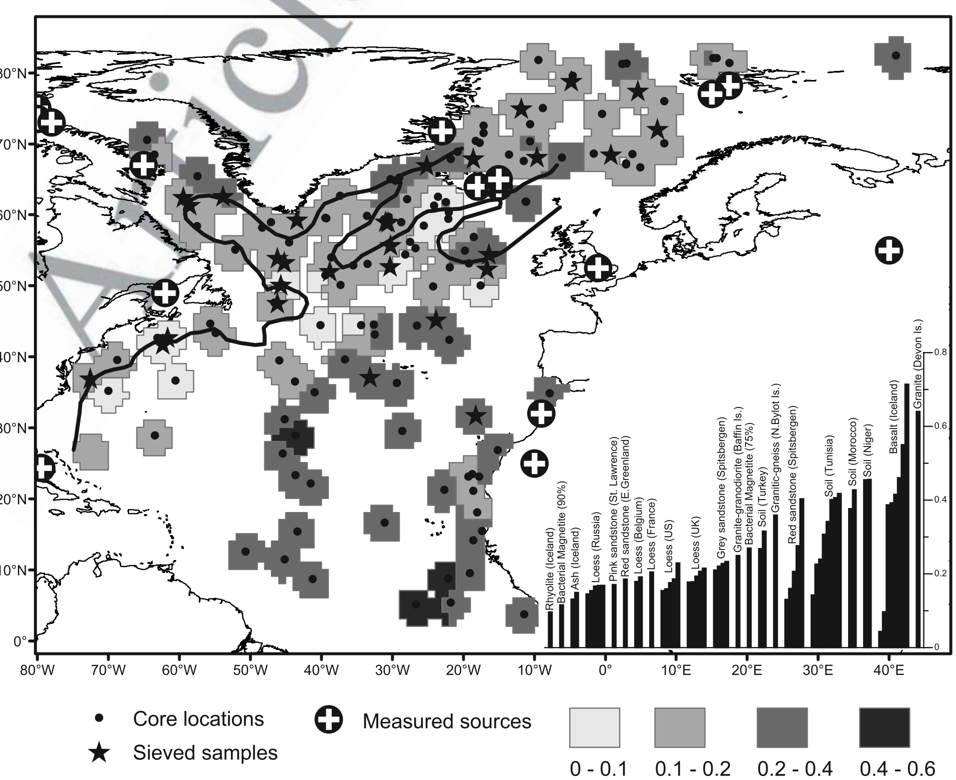

Figure 8. Low field remanence (IRM_{20mT}/IRM_{100mT}) values in LGM North Atlantic deep-sea sediments and a range of potential source samples.

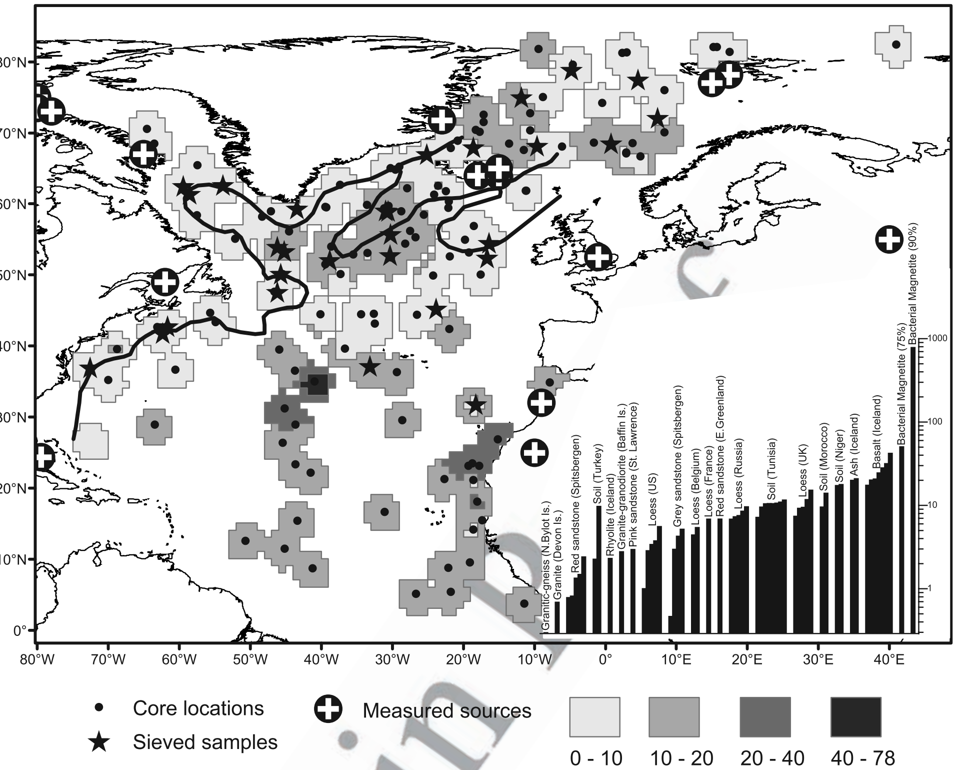

Figure 9. Anhysteretic remanence (normalized to magnetic susceptibility, χ_{ARM}/χ_{lf}) values in LGM North Atlantic deep-sea sediments and a range of potential source samples.

magnetically hard, lithogenic single domain-like ferrimagnets. Low to intermediate values are found to the south of Iceland and throughout the Nordic Seas, together with moderate to high χ_{lf} values. Figure 9 shows the sediment anhysteretic remanence (normalized to magnetic susceptibility, χ_{ARM}/χ_{lf}, another indicator of magnetic grain size, sensitive to the presence of ultrafine magnetic grains close to the single domain/superparamagnetic boundary) together with values of this parameter for our potential sources. For the LGM sediments, areas of highest anhysteretic remanence values are composed of the aeolian dust-dominated samples to the west of Africa, and parts of the Nordic Seas and the area south of Greenland.

[24] The individual magnetic parameter plots thus reveal evidence of distinctive spatial patterns of sediment magnetic properties across the North Atlantic LGM sediment surface, and appear to be indicative of different terrigenous magnetic sources. Principally, we infer on a whole ocean basis, North Atlantic glacial sediments are magnetically dominated at low latitudes (to ~30N) by aeolian dust, and at high latitudes and midlatitudes by IRD, especially in the Nordic Seas and the central North Atlantic, but also extending as far south as ~32N. Even along the major deep water trajectories, significantly different sediment magnetic properties are observed. Previously, little magnetic change (other than changes in magnetic concentration) has been interpreted for some glacial sediments along the path of the NADW [e.g., *Kissel*, 2005]. We summarize these differences in the magnetic properties of the North Atlantic sediments at the LGM and the present day below, following statistical analysis of the magnetic data.

[25] The LGM North Atlantic sediment magnetic properties contrast markedly with those at the present day. Not only was more detrital magnetic material delivered to the ocean at the LGM, especially to large areas of the central North Atlantic region, but, for much of the ocean, including the entire area spanning the Nordic Seas and the eastern North Atlantic (east of ~30W, south of ~55N), the magnetic mineralogy supplied was significantly different from that at present. These data suggest that the LGM North Atlantic circulation was very different from that at present. Notably, the transport and survival of icebergs to the central North Atlantic zone to the west of the U.K. and even further south indicates a weakened, southerly displaced North Atlantic Current (NAC), and thus significant reduction in NADW formation at the LGM.

3.3. Fuzzy Clustering of Magnetic Data

[26] In a first attempt to obtain objective identification of sediment magnetic groupings and possible transport pathways, fuzzy c means clustering and nonlinear mapping (NLM) were applied to the magnetic data sets. The fuzzy c-means cluster performance is indicated by two statistics, the partition coefficient, *F* and classification entropy, H. The "best" clustering solution (as indicated by the highest F and lowest H) for the magnetic data set for the LGM North Atlantic sediments was achieved initially with three clusters. One of the clusters, occurring only to the west of Africa and south of 50N (Figure 10), is characterized by SP ferrimagnets and high-coercivity minerals, like haematite. This

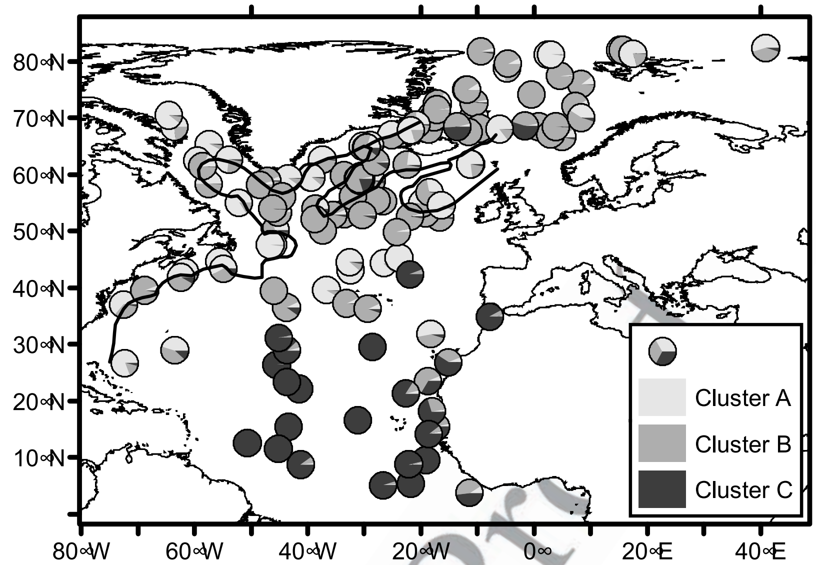

Figure 10. Classification of LGM sediment sample magnetic data by fuzzy clustering: the three-cluster solution; cluster C is samples magnetically dominated by aeolian dust.

cluster reflects the deposition of African, soil-derived dust. The two remaining clusters populate the northern and western North Atlantic and are characterized by the presence of coarser ferrimagnets (i.e., of lithogenic rather than soil-formed origin). To provide improved differentiation between these two latter clusters, the dust-dominated samples were removed from the data set and the clustering procedure rerun on the remaining data (112 sediment samples). The "best" clustering solution for this data set was achieved with six clusters. The parameter means for each of the six clusters are shown in Table 3. The NLM (Figure 11), a two-dimensional projection of the multidimensional data [*Vriend et al.*, 1988], indicates that four of the clusters (1, 2, 3 and 4) are well separated (i.e., display large interdata distance). The remaining two clusters (5 and 6) are well separated from the other clusters but overlap with each other. Samples dominated magnetically by finer-grained lithogenic ferrites plot in the upper section of the NLM, those dominated by coarse-grained ferrites in the lower left section, and those by high-coercivity (haematite-like) minerals to the right of the NLM. The highest number of sediment samples group within clusters 3, 4, 5, and 6.

[27] These statistical groupings derive only from the measured magnetic properties for each sediment sample; no geographic information was used in their definition. The spatial dimension can subsequently be examined by plotting each sediment sample by location as well as statistical cluster membership. Figure 12 shows the fuzzy clustering results for the LGM sediments, with the pie diagram for each sample indicating its degree of affinity with each of the clusters (ranging from 0 equals no affinity to 1 indicates identical to the cluster mean). Sediments which are dominantly characterized by single-cluster membership, can be identified; conversely, sediments which appear to represent mixtures of magnetic types are also evident. Figures 13–17 show the samples by location and, where appropriate, their dominant cluster membership; that is, samples are classified

Table 3. Cluster Means for the Six-Cluster Solution (After Removal of the Dust-Dominated Samples)

	Cluster					
	1	2	3	4	5	6
χ_{fd}, %	1.25	1.41	1.84	2.90	3.70	4.30
HIRM, %	10.57	4.61	1.54	5.44	3.31	3.92
χ_{ARM}/χ_{lf}	4.44	4.30	4.30	8.71	9.31	12.00
IRM_{20mT}/IRM_{100mT}	0.13	0.22	0.20	0.20	0.12	0.18

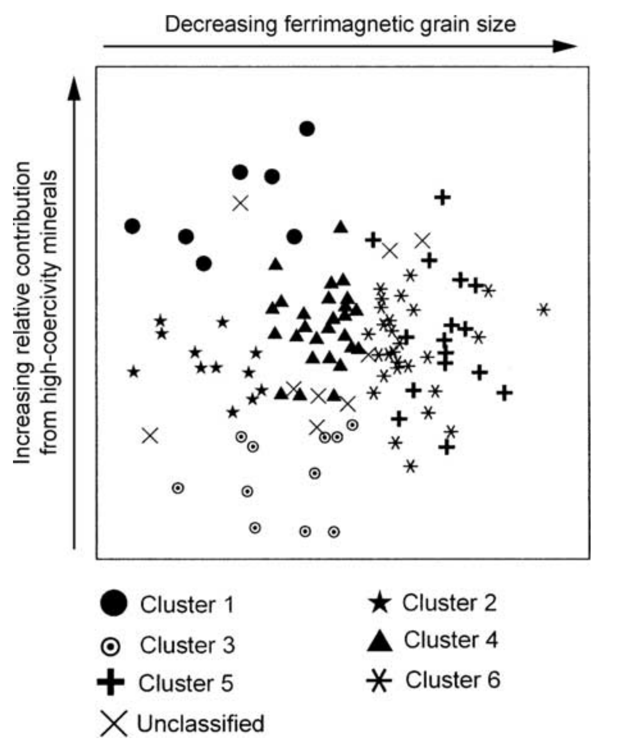

Figure 11. Nonlinear mapping (NLM) for the six-cluster solution (with dust-dominated samples removed).

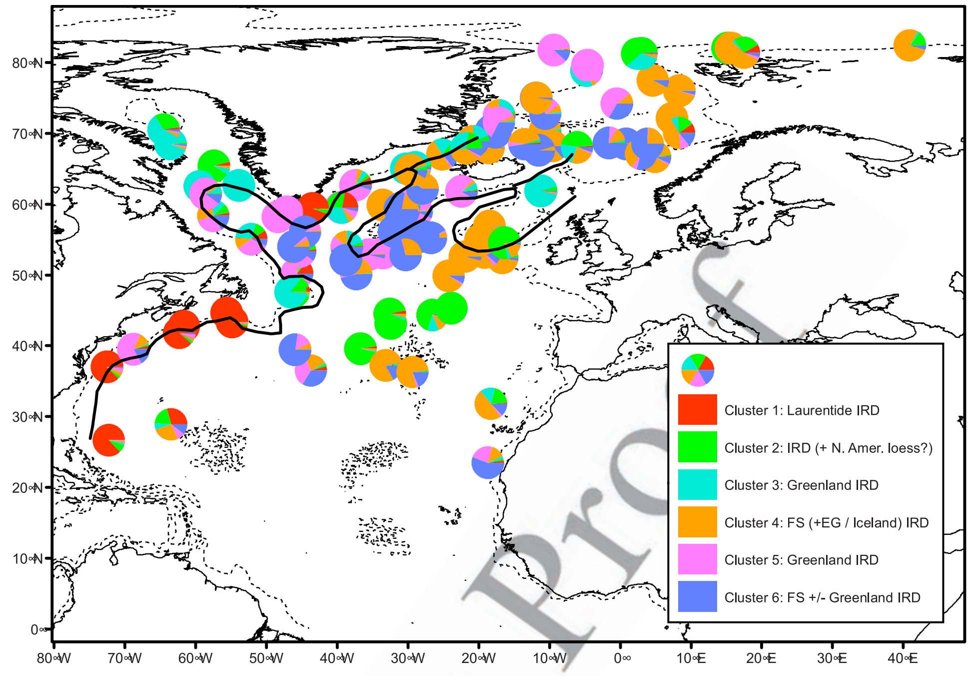

Figure 12. Classification of LGM sediment samples by fuzzy clustering: the six-cluster solution, with the dust-dominated samples removed from the cluster analysis. The degree of affinity to each of the identified clusters is shown as a pie chart for each sample. FS is Fennoscandian; EG is East Greenland.

as “belonging” to a particular cluster when the ratio of the highest membership to the second highest membership is >0.75; if this condition is not satisfied, the sample is unclassified [*Hanesch et al.*, 2001]. Table 4 summarizes the magnetic clustering information, spatial distributions and possible sources for the LGM sediment samples. IRD was previously reported in North Atlantic samples as far south as 37N [*Baas et al.*, 1997]. Here we identify IRD at

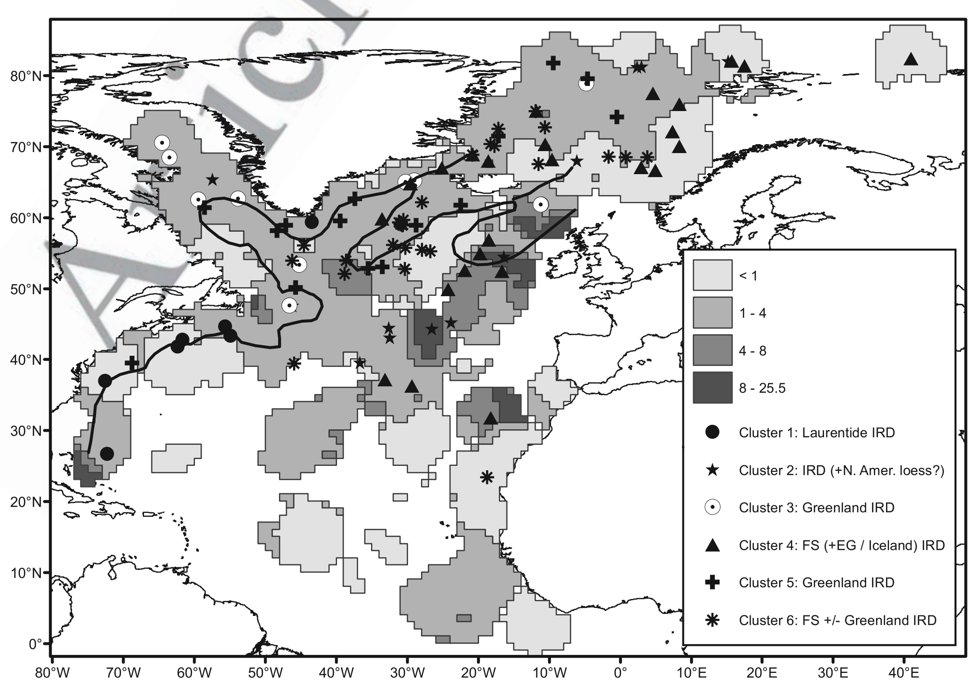

Figure 13. Spatial distribution of cluster membership for the six-cluster solution (with dust-dominated samples removed). The size of the cluster symbol is proportional to the strength of the sample membership to that cluster. The NADW trajectory [*Kissel et al.*, 1997] is shown, together with the ratio of χ_{lf} ($\times 10^{-6}$ m^3 kg^{-1}) at the LGM compared to the present day. FS is Fennoscandian; EG is East Greenland.

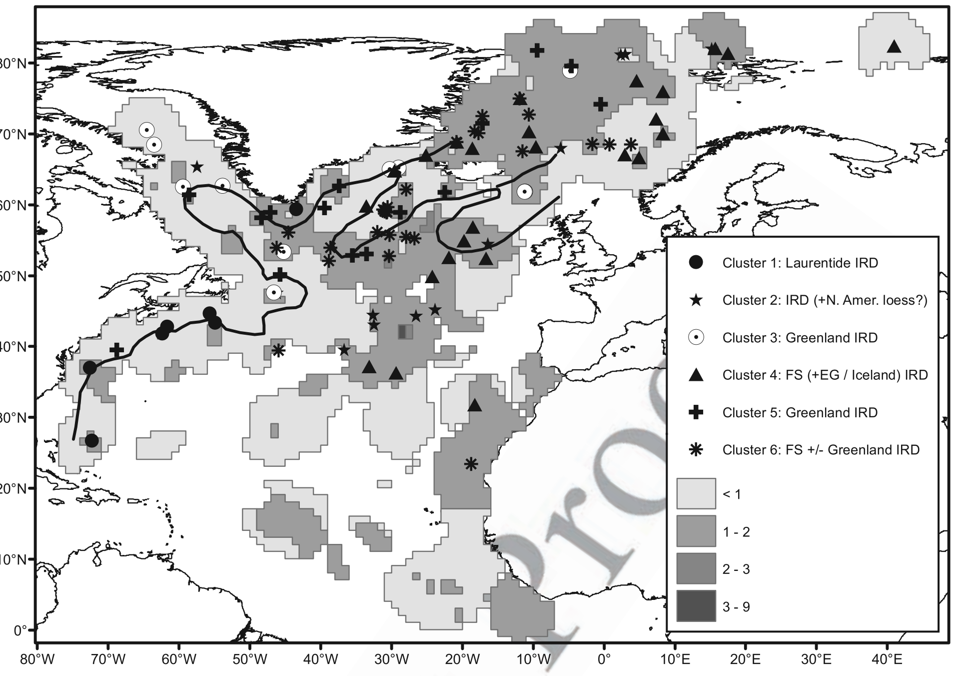

Figure 14. Classification of LGM sediment samples by fuzzy clustering, together with the ratio of $IRM_{20-100mT}/IRM_{100mT}$ at the LGM compared to the PD. FS is Fennoscandian; EG is East Greenland. Values >1 indicate enhanced input of single-domain/pseudosingle-domain-like ferrimagnetic particles at the LGM. Significant increases at the LGM in this "intermediate" remanence fraction (i.e., the proportion of the remanence acquired between 20 and 100 mT applied field) are seen across a very large portion of the northeastern and central North Atlantic, showing significantly different detrital ferrimagnetic input from that at the present day.

even lower latitudes of ~32N, 18W (and confirm its presence by sieving to reveal detrital grains >150 μm [*Watkins*, 2003] (see also auxiliary material)).

[28] In summary, magnetic characterization of North Atlantic LGM sediments, together with a range of potential source samples, identifies distinct and statistically robust regionalization or spatial groupings of sediments, with magnetic signatures dominated (i.e., on a whole ocean basis) either by inputs of IRD or aeolian dust, according to latitude. It should be noted again that we use the magnetic signature as a tracer, or "fingerprint," not as an indicator of sediment volume (often dominated by biogenic carbonate, for example) or magnetic concentration. After removal of the aeolian-dominated samples, the sediments can be split statistically into six different clusters based on their magnetic signatures. The great majority of these samples appear to contain IRD from three principal sources: Fennoscandia (plus East Greenland and Iceland); Greenland; and the St. Lawrence region. Fennoscandian-sourced IRD seems dominant in the central and NE North Atlantic. Greenland-sourced material is concentrated in the north and NW North Atlantic, while the St. Lawrence-sourced detrital magnetic components appear mainly restricted to the eastern seaboard of North America, with some possible extension toward the central North Atlantic. Across major swathes of the North Atlantic, the LGM sediment magnetic properties contrast markedly with those at the present day. Sediment transport and redistribution by bottom water processes cannot explain the ocean-wide distributions of these different sediment magnetic signatures. Paths of bottom water flow, limited to linear and spatially limited ocean areas, show negligible relationship with either the LGM/present-day difference patterns or our mapped statistical groupings (Figures 13–15). To test further any possible influence of bottom water transport, we can remove from the LGM data set any sample within the bottom water realm, and rerun the fuzzy clustering. The remaining pelagic samples group into similar clusters and spatial distributions, indicating the bottom-water-located samples play no significant role in determining the ocean-wide spatial patterns. Conversely, running cluster analysis only on bottom water zone samples results in clusters with similar means and spatial distributions to the whole sample set analysis. LGM sediments display statistically different magnetic mineralogical properties along the NADW trajectory, and demonstrably contain coarse particles of IRD origin (see auxiliary material). Our future studies will examine independently these magnetically based IRD groupings, through the use of high-resolution, paired magnetic and isotope geochemical signatures of IRD in North Atlantic sediments, and its potential sources.

4. Discussion

[29] On the basis of the magnetic signatures of 112 sediment samples (37 pelagic and 75 hemipelagic) distributed across the North Atlantic; their contrast with present-day sediment magnetic signatures; matching of the LGM

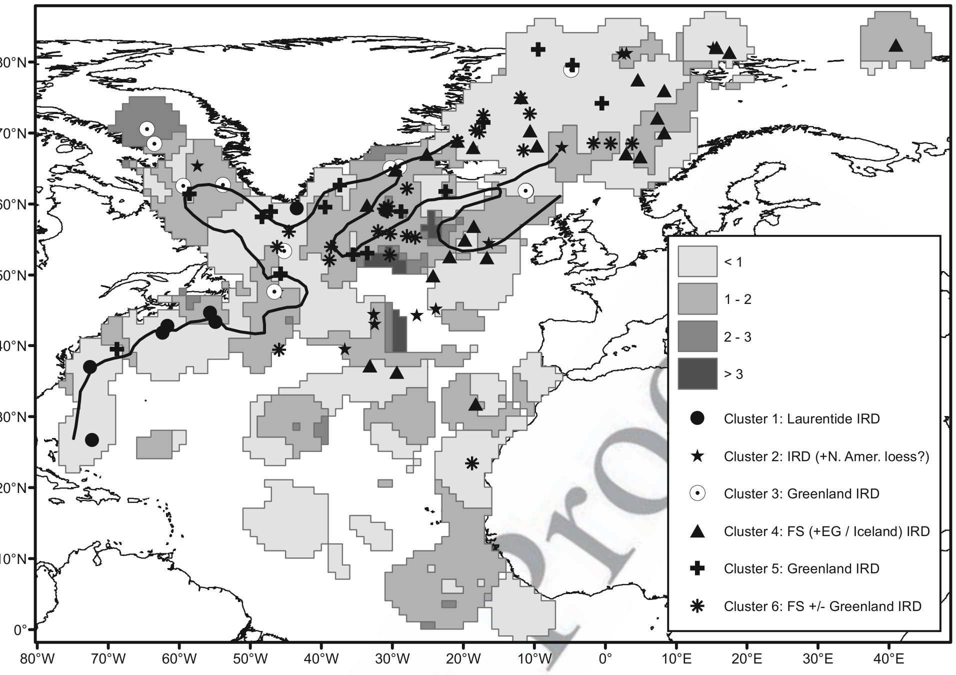

Figure 15. Classification of LGM sediment samples by fuzzy clustering, together with the ratio of "soft" magnetic remanence ratio (IRM_{20mT}/IRM_{100mT}) at the LGM compared with the PD. FS is Fennoscandian; EG is East Greenland. Ratios were calculated by interpolating LGM and PD values to a 1 × 1 grid. Values >1 indicate enhanced input of either coarse, multidomain-like magnetic particles (especially when associated with low values of frequency-dependent susceptibility) or magnetically unstable (viscous) grains at the fine-grained/ultrafine-grained (single domain/superparamagnetic) boundary (especially when associated with high values of frequency-dependent susceptibility).

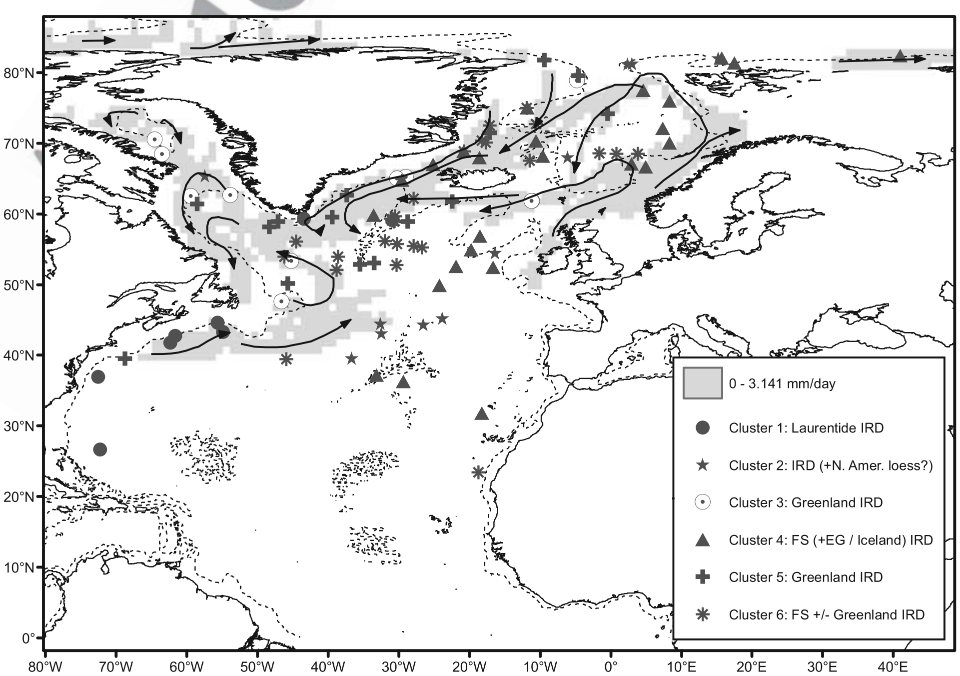

Figure 16. Comparison between the predicted iceberg trajectories and the IRD clusters for the NSS model. FS is Fennoscandian; EG is East Greenland.

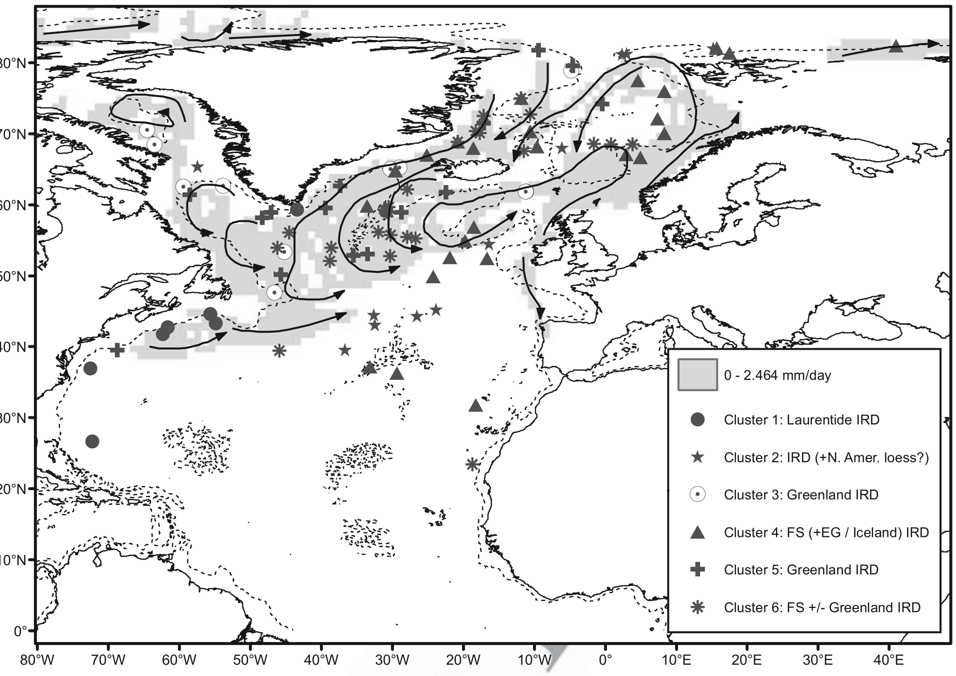

Figure 17. Comparison between the predicted iceberg trajectories and the IRD clusters for the SSS model. FS is Fennoscandian; EG is East Greenland.

and present-day magnetic signatures with a range of circum-Atlantic potential source materials; and the near ubiquity of coarse-grained material (>150 μm in size, i.e., unambiguously of IRD origin) within our samples, we suggest there are distinct, ocean-wide groupings of LGM IRD distributions and sources.

[30] Using these inferred IRD types and distributions, we can test our three modeled ocean circulation states spanning the range of likely or possible LGM ocean circulations. Figures 16–18 show the predicted iceberg contribution to meltwater for each modeled state, together with our interpreted clusters. Of our modeled states, only the SSS (Figure 17) can match the spatial distribution of many of the IRD-related clusters. This is especially so for the region west of the United Kingdom, where only the SSS can account for the survival and transport of (probably Fennoscandian sourced) icebergs to the latitude of the cluster 4 samples. Additionally, around the Greenland coast, the distribution of strongly magnetic cluster 3 and 5 samples is most closely matched by the SSS modeled iceberg trajectories, which indicate only southward flow of Green-

Table 4. Summary of Magnetic Cluster Data for LGM North Atlantic Sediment Samples

Cluster	Sample Set, %	Distribution	Magnetic "Fingerprint"	Possible Sources
1	6	restricted to east coast North America, ~30–50N	highest HIRM (10.6%) and lowest χ_{fd} (1.3%)	glacially derived, haematite-rich input (plus/minus any bottom water reworking), e.g., St. Lawrence region; iceberg melting near coast
2	11	central North Atlantic, 60–25W and 40–50N; isolated samples Labrador Sea, northern Nordic Seas	Low χ_{fd} (1.4%), lowest χ_{ARM}/χ_{lf} (4.3), HIRM third highest (4.6%), highest IRM_{20mT}/IRM_{100mT} (0.22)	?far traveled IRD from St. Lawrence region (central North Atlantic samples); red beds of circum–Norwegian Sea, e.g., Spitsbergen, Greenland; cluster means also similar to North American loesses
3, 5	25	restricted to north and west North Atlantic, along Greenland coast, around Iceland, throughout Labrador Sea and Baffin Bay	lowest HIRM (1.5%), low χ_{fd} (1.8%), high IRM_{20mT}/IRM_{100mT} (0.2) suggesting coarse, MD-like lithogenic ferrimagnets; χ_{ARM}/χ_{lf}, χ_{fd} and HIRM means for cluster 5 slightly higher than cluster 3	Icelandic basaltic source rocks, Precambrian igneous rocks and Tertiary basalts, Greenland and Labrador coast; admixed Icelandic ash and/or haematite-rich IRD, e.g., Fleming Fjord, required to account for cluster means
4	25	wide distribution eastern North Atlantic, mostly E of 40W; as far south as 32N; highest affinities, East Greenland, W of U. K., parts Nordic Seas	χ_{ARM}/χ_{lf} higher than clusters 1–3 (8.7), χ_{fd} 2.9%, IRM_{20mT}/IRM_{100mT} values relative high (0.2); HIRM moderate (5%)	IRD dominated by SD/PSD magnetite, admixture of haematite-containing source rocks, e.g., northern Spitsbergen, western Scotland, East Greenland
6	25	SW Iceland (~30–40W, 50N), south of Greenland at ~45W and along the southern margin of the Nordic Seas (~67N).	highest χ_{ARM}/χ_{lf} (12) and χ_{fd} (4.3%), relative high IRM_{20mT}/IRM_{100mT} (0.18), moderate HIRM (3.9%)	high > 150 μm % values, significant IRD input, basaltic-rich IRD from Greenland plus or minus Icelandic igneous provinces

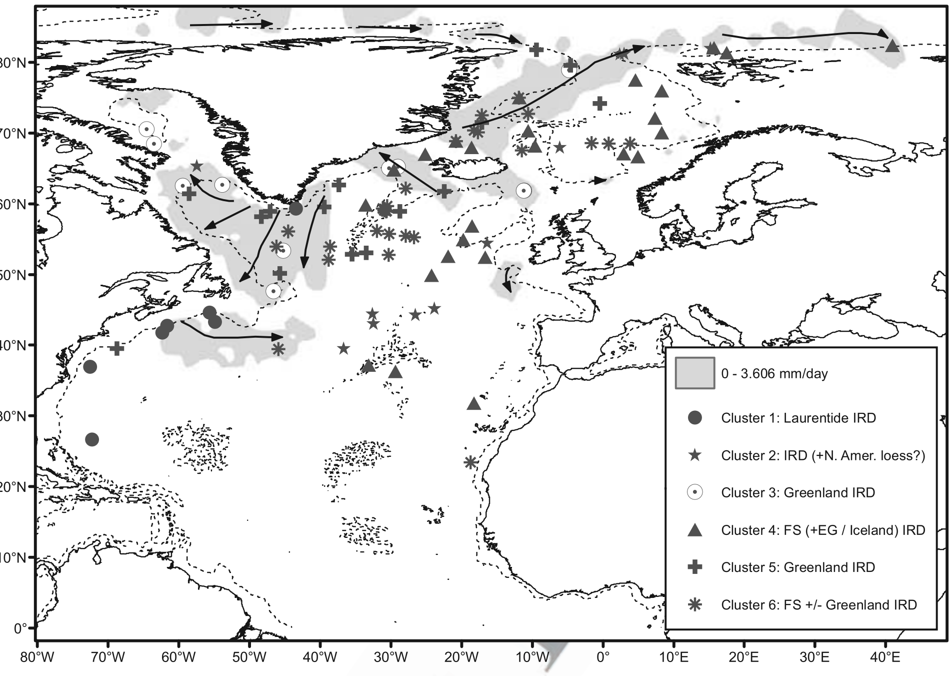

Figure 18. Comparison between the predicted iceberg trajectories and the IRD clusters for the ISS model. FS is Fennoscandian; EG is East Greenland.

land-sourced icebergs in the Labrador Sea. Such flow is supported by the surface current reconstructions of *Ruddiman* [1977], *Fillon et al.* [1981] and *Stoner et al.* [1996]. In contrast, the NSS transports St. Lawrence icebergs northward. These icebergs would be expected to contain a significant amount of haematite-rich IRD from the St. Lawrence red beds, yet there is no northward extension of cluster 1 samples (St. Lawrence IRD) or of high HIRM values (Figure 7). *de Vernal et al*'s [2005] sea surface condition reconstruction for the northern Atlantic suggests that northward advection of water into the Labrador Sea almost stopped during the LGM.

[31] Despite the otherwise close match of the SSS iceberg trajectories with the inferred Fennoscandian IRD patterns, none of the circulation states can produce iceberg trajectories matching the eastward extent of St. Lawrence IRD (inferred as a possible source for cluster 2 samples in the central North Atlantic). This easterly extent is most closely matched by the NSS (Figure 16). Validation of the iceberg model for the present day indicates that the model melts icebergs too quickly in some regions [*Gladstone et al.*, 2001]. If iceberg melting is turned off, some St. Lawrence icebergs are transported to this region in both the NSS and SSS. Additionally, the SSS and ISS can transport Greenland and Fennoscandian icebergs to this region (cluster memberships in this region suggest that the most easterly of these samples have a significant Fennoscandian IRD contribution). It is possible that samples in this region, together with additional IRD samples south of ~45N, which cannot be explained by any model state, may represent southward (infrequent and extreme) iceberg trajectories not represented by the averaged forcing fields of the iceberg model. Alternatively, such samples indicate that the real LGM circulation did not match any of our three modeled possibilities.

[32] The modeled SSS circulation is dominated by formation of deep water in the Southern Ocean, with additional formation of intermediate depth water in the North Atlantic, but at a low rate. Such a circulation state is consistent with reconstructions of LGM ocean circulation based on δ^{13}C measurements [e.g., *Oppo and Fairbanks*, 1987; *Michel et al.*, 1995]. Greater penetration of southern-sourced deep water during the LGM is a common feature of many models and proxy data reconstructions [e.g., *Sarnthein et al.*, 1994, 1995; *Beveridge et al.*, 1995; *Seidov and Haupt*, 1997; *Ganopolski et al.*, 1998]. However, the current "most favored" LGM circulation state [*Boyle and Keigwin*, 1987; *Sarnthein et al.*, 1994, 1995; *Beveridge et al.*, 1995; *Seidov and Haupt*, 1997; *Ganopolski et al.*, 1998] has much stronger production of intermediate depth water in the North Atlantic than the SSS. The OGCM that produces the ISS is consistent with this state [*Wadley et al.*, 2002]. While the ISS iceberg trajectories (Figure 18) are similar to those of the SSS south of Greenland, they are unable to explain the widespread distribution of IRD clusters, especially in the region south of Iceland (even with iceberg melting turned off). It is possible that some combination of the SSS and ISS circulation is the best approximation of the LGM circulation (e.g., the SSS but with a stronger rate of deeper, intermediate water formation and a shift in its location in the SSS state from west of Africa to the region south of Iceland). Such a shift is possible if the background salinity of the region south of Iceland were higher because of more northerly penetration of a branch of the salty NAC, as *de Vernal et al.* [2005] suggest. However, this would need to be relatively narrow and confined to the eastern Atlantic to be consistent with the magnetic data (otherwise icebergs would melt before reaching their identified more southerly extents).

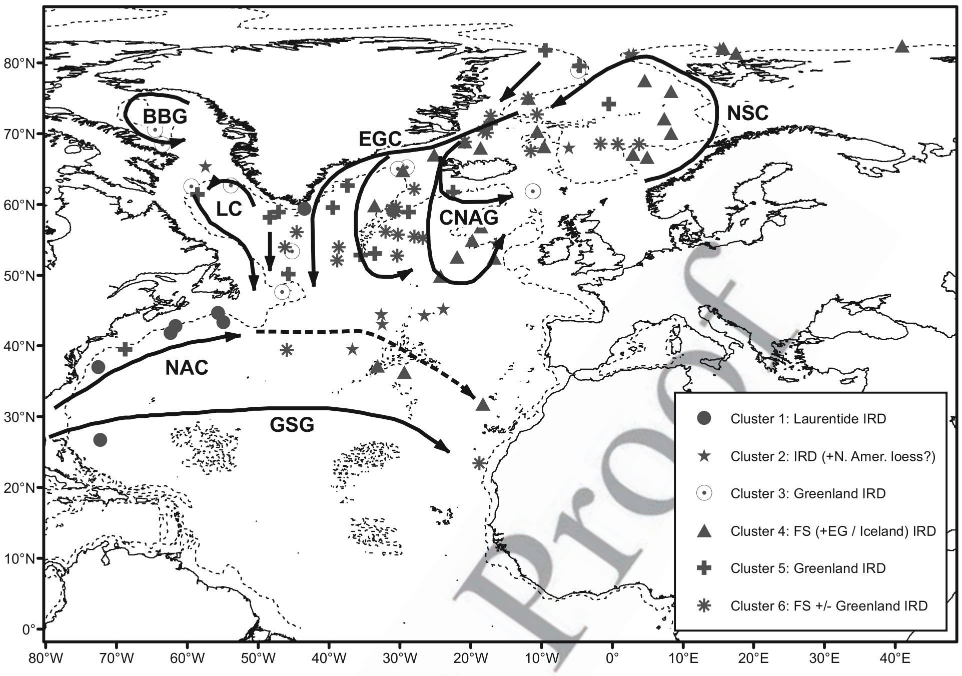

Figure 19. Reconstructed surface circulation patterns based on the IRD clusters and the SSS iceberg results. Abbreviations are NSC, Norwegian Sea Current; EGC, East Greenland Current; CNAG, central North Atlantic gyre; BBG, Baffin Bay gyre; LC, Labrador Current; NAC, North Atlantic Current; GSG, glacial subtropical gyre; FS, Fennoscandian; and EG, East Greenland. It is possible that the NAC also had a narrow, northeasterly branch, feeding warmer waters toward the eastern Nordic Seas.

[33] Using the magnetically based cluster data, a surface circulation pattern can be reconstructed for the LGM (Figure 19). Its main feature is a gyre south of Iceland, the Central North Atlantic Gyre (CNAG), fed by the East Greenland Current (EGC) and the Norwegian Sea Current (NSC). This gyre transports Fennoscandian and East Greenland icebergs around a mid-Atlantic zone, with most IRD deposition at the high magnetic susceptibility zone (Figure 13) west of the United Kingdom. This reconstruction differs from that of *Robinson et al.* [1995], who suggested entrainment within the CNAG of icebergs sourced from Baffin Bay, the Labrador Sea and the St. Lawrence region. It also differs from the transfer-function-based reconstructions for the GLAMAP and EPILOG time slices (18–22 kyr B.P. and 19–23 kyr B.P., respectively), which indicate a midlatitude anticyclonic gyre, transporting warm waters as far north as Iceland [e.g., *Pflaumann et al.*, 2003]. It is similar to that of the CLIMAP group [*McIntyre et al.*, 1976], which featured a latitudinally compressed and longitudinally expanded cyclonic gyre south of Iceland, separated from the NAC. Such radically differing circulation reconstructions are not unexpected given not only our new IRD data but also significant differences in published LGM sea surface temperatures (SSTs) and sea ice extent [*Byrkjedal et al.*, 2006]. For example, SST reconstructions by *Meland et al.* [2005] for the Nordic Seas, based on planktic foraminiferal oxygen isotopes, differ significantly from those of *Pflaumann et al.* [2003], with lower temperatures and a significant east-west temperature gradient with warmer temperatures in the eastern Nordic Seas. *Meland et al.* [2005] infer inflowing warmer waters in the eastern North Atlantic and a compensating southward flow of colder Polar waters off east Greenland (see, for comparison, our Figure 19). The GLAMAP, EPILOG, CLIMAP and our reconstruction all identify a similar path for the LGM NAC, flowing eastward with a northerly limit of ~40–42N, with a branch to the south, accounting for our observation of IRD at our most southerly latitude, ~32N, off the NW African coast. The more zonal nature of the NAC is a result of the southward extension of the Laurentide ice sheet, which modified the strength and circulation pattern of the North Atlantic westerly jet [*Seidov and Haupt*, 1997; *Pailler and Bard*, 2002].

[34] Early reconstructions of the last glacial (25–13 kyr B.P.) circulation by, for example, *Fillon et al.* [1981] and the LGM circulation by *Robinson et al.* [1995] suggested that the dominant IRD source in the North Atlantic was the Hudson Strait/Labrador Sea region. In contrast, Fennoscandian- and Greenland-derived icebergs form the dominant source of IRD N of 50N in our reconstruction. Additional evidence for the importance of LGM Fennoscandian sources comes from reconstructed circulation patterns, petrological and isotopic analysis of sediments [e.g., *Ruddiman*, 1977; *Grousset et al.*, 1993; *Sarnthein et al.*, 1995; *Revel et al.*, 1996; *Rasmussen et al.*, 1997; *Richter et al.*, 2001; *Auffret et al.*, 2002; *Peck et al.*, 2006]. With regard to the Laurentide ice sheet, the magnetic, modeling and the sediment carbonate results (Figure 4) presented here all suggest a minor role for Hudson Strait IRD (which does not exit from the Labrador Sea in any of the three states used here)

and slightly greater significance of St. Lawrence-sourced icebergs.

5. Conclusions

[35] On the basis of our magnetic and modeling data, we draw the following conclusions.

[36] 1. The sediments of the LGM North Atlantic can be characterized magnetically, to identify a low-latitude zone magnetically dominated by aeolian sources, and a high-latitude to midlatitude zone magnetically dominated by strongly magnetic, nonaeolian, detritral sources.

[37] 2. We infer, from comparisons between the LGM sediment magnetic properties and a range of potential circum-Atlantic source rocks, and the LGM and present-day sediment magnetic properties, and from grain size analysis, that iceberg rafting was a major source of magnetic input across much of the high-latitude to midlatitude glacial North Atlantic, even extending to sediments as far south as 32N.

[38] 3. Magnetic parameters, used to infer North Atlantic IRD patterns and sources, indicate two major IRD sources, Fennoscandia and Greenland/Iceland, and one minor source, the St. Lawrence region.

[39] 4. Of the three modeled LGM ocean circulation states described here, the modeled iceberg trajectories of the SSS most closely match our reconstructed IRD patterns. This modeled circulation state is characterized by dominant formation of deep water in the Southern Ocean. However, it is possible that some combination of the SSS and ISS circulation is the best approximation of the LGM circulation, with additional intermediate water formation in the central North Atlantic. This shift is possible if the background salinity of the region south of Iceland was higher because of more northerly penetration of an eastern branch of the salty NAC.

[40] 5. The SSS trajectories and magnetic results indicate that the LGM surface circulation was dominated by a cyclonic Central North Atlantic Gyre, which delivered significant numbers of Fennoscandian (plus East Greenland and Icelandic) icebergs to the North Atlantic. This gyre was separated from the NAC, which was displaced south of ∼42N.

[41] 6. The magnetic data indicate that Fennoscandian-sourced IRD dominated the LGM across much of the North Atlantic region.

[42] 7. In terms of the Laurentide ice sheet, the Hudson Strait IRD contribution appears, from our data, to be very minor, with St. Lawrence–sourced IRD of slightly greater importance.

[43] 8. The sediment magnetic data also identify those areas of the North Atlantic magnetically dominated by aeolian deposition of dust from Africa.

[44] **Acknowledgments.** This work was carried out under a Natural Environment Research Council Ph.D. studentship (04/99/ES/62). We thank the following for access to deep-sea sediment samples: I. Hardy, Canadian Geological Survey; M. Sarnthein, Kiel University; G. Rothwell, Southampton University; L. Keigwin, J. Broda, and E. Roosen, Woods Hole Oceanographic Institute; A. de Vernal and G. Bilodeau, University of Quebec at Montreal; J. Matthiessen and M. Pirrung (now at Jena), AWI-Bremerhaven; J. Andrews, INSTAAR, University of Colorado; B. Balsam, University of Texas at Arlington; T. Richter, Netherlands Institute for Sea Research, Netherlands; and M. Moros, University of Bergen. M. Dekkers (Utrecht) kindly made available the fuzzy cluster software. Martin Wadley (University of East Anglia) assisted with providing the model ocean circulation fields. We appreciate the helpful comments of the two reviewers.

References

Andrews, J. T., T. A. Cooper, A. E. Jennings, A. B. Stein, and H. Erlenkeuser (1998), Late Quaternary iceberg-rafted detritus events on the Denmark Strait–southeast Greenland continental slope (∼65N): Related to N. Atlantic Heinrich events?, *Mar. Geol.*, *149*, 211–228.

Auffret, G., S. Zaragosi, B. Dennielou, E. Cortijo, D. van Rooij, F. Grousset, C. Pujol, F. Eynaud, and M. Siegert (2002), Terrigenous fluxes at the Celtic margin during the last glacial cycle, *Mar. Geol.*, *188*, 79–108.

Balsam, W. L., and F. W. McCoy (1987), Atlantic sediments: Glacial/interglacial comparisons, *Paleoceanography*, *2*, 531–542.

Balsam, W. L., B. L. Otto-Bliesner, and B. C. Deaton (1995), Modern and Last Glacial Maximum eolian sedimentation patterns in the Atlantic Ocean interpreted from sediment iron oxide content, *Paleoceanography*, *10*, 493–507.

Baas, J. H., J. Mienert, F. Abrantes, and M. A. Prins (1997), Late Quaternary sedimentation on the Portuguese continental margin: Climate-related processes and products, *Palaeogeogr. Palaeoclimatol. Palaeoecol.*, *130*, 1–23.

Beveridge, N. A. S., H. Elderfield, and N. J. Shackleton (1995), Deep thermohaline circulation in the low-latitude Atlantic during the last glacial, *Paleoceanography*, *10*, 643–660.

Bigg, G. R., and M. R. Wadley (2001), The origin and flux of icebergs released into the Last Glacial Maximum Northern Hemisphere oceans: The impact of ice sheet topography, *J. Quat. Sci.*, *16*, 565–573.

Bigg, G. R., M. R. Wadley, D. P. Stevens, and J. A. Johnson (1996), Prediction of iceberg trajectories for the North Atlantic and Arctic oceans, *Geophys. Res. Lett.*, *23*, 3587–3590.

Bigg, G. R., M. R. Wadley, D. P. Stevens, and J. A. Johnson (1997), Modelling the dynamics and thermodynamics of icebergs, *Cold Reg. Sci. Technol.*, *26*, 113–135.

Bigg, G. R., M. R. Wadley, D. P. Stevens, and J. A. Johnson (1998), Simulations of two Last Glacial Maximum ocean states, *Paleoceanography*, *13*, 340–351.

Bond, G., W. Showers, M. Cheseby, R. Lotti, P. Almasi, P. deMenocal, P. Priore, H. Cullen, I. Hajdas, and G. Bonani (1997), A pervasive millennial-scale cycle in North Atlantic Holocene and glacial climates, *Science*, *278*, 1257–1266.

Boyle, E. A., and L. Keigwin (1987), North Atlantic thermohaline circulation during the past 20,000 years linked to high-latitude surface temperature, *Nature*, *330*, 35–40.

Byrkjedal, O., N. Kvamsto, M. Meland, and E. Jansen (2006), Sensitivity of Last Glacial Maximum climate to sea ice conditions in the Nordic Seas, *Clim. Dyn.*, *26*, 473–487.

Cremer, M., F. Grousset, J. C. Faugeres, J. Duprat, and E. Gonthier (1992), Sediment flux patterns in the northeastern Atlantic: Variability since the last interglacial, *Mar. Geol.*, *104*, 31–53.

Dearing, J. A., R. J. L. Dann, K. Hay, J. A. Lees, P. J. Loveland, B. A. Maher, and K. O'Grady (1996), Frequency-dependent susceptibility measurements of environmental materials, *Geophys. J. Int.*, *124*, 228–240.

de Vernal, A., and C. Hillaire-Marcel (2000), Sea-ice cover, sea-surface salinity and halo-/thermocline structure of the northwest North Atlantic: Modern versus full glacial conditions, *Quat. Sci. Rev.*, *19*, 65–85.

de Vernal, A., et al. (2005), Reconstruction of sea-surface conditions at middle to high latitudes of the Northern Hemisphere during the Last Glacial Maximum (LGM) based on dinoflagellate cyst assemblages, *Quat. Sci. Rev.*, *24*, 897–924.

Dong, B., and P. J. Valdes (1998), Simulations of the Last Glacial Maximum climates using a general circulation model: Prescribed versus computed sea surface temperatures, *Clim. Dyn.*, *14*, 571–591.

Duplessy, J.-C., J. Moyes, and C. Pujol (1980), Deep water formation in the North Atlantic Ocean during the last ice age, *Nature*, *286*, 479–481.

ETOPO5 (1986), Global $5' \times 5'$ depth and elevation, http://www.ngdc.noaa.gov/mgg/global/

etopo5.HTML, Natl. Geophys. Data Cent., Boulder, Colo.
Fairbanks, R. G. (1989), A 17,000 year glacio-eustatic sea-level record: Influence of glacial melting rates on the Younger Dryas event and deep-ocean circulation, *Nature*, *342*, 637–642.
Farmer, G. L., D. Barber, and J. Andrews (2003), Provenance of late Quaternary ice-proximal sediments in the North Atlantic: Nd, Sr and Pb isotopic evidence, *Earth Planet. Sci. Lett.*, *209*, 227–243.
Fillon, R. H., G. H. Miller, and J. T. Andrews (1981), Terrigenous sand in Labrador Sea hemipelagic sediments and paleoglacial events on Baffin Island over the last 100,000 years, *Boreas*, *10*, 107–124.
Ganopolski, A., S. Rahmstorf, V. Petoukhov, and M. Claussen (1998), Simulation of modern and glacial climates with a coupled model of intermediate complexity, *Nature*, *391*, 351–356.
Gladstone, R. M. (2001), A modelling and remote sensing study of Antarctic icebergs, Ph.D. thesis, School of Environ. Sci., Univ. of East Anglia, Norwich, U. K.
Gladstone, R. M., G. R. Bigg, and K. W. Nicholls (2001), Iceberg trajectory modeling and meltwater injection in the Southern Ocean, *J. Geophys. Res.*, *106*, 19,903–19,915.
Grousset, F. E., L. Labeyrie, J. A. Sinko, M. Cremer, G. Bond, J. Duprat, E. Cortijo, and S. Huon (1993), Patterns of ice-rafted detritus in the glacial North Atlantic (40–55N), *Paleoceanography*, *8*, 175–192.
Hall, N. M. J., P. J. Valdes, and B. W. Dong (1996), The maintenance of the last great ice sheets: A UGAMP GCM, *J. Clim.*, *9*, 1004–1019.
Hanesch, M., R. Scholger, and M. J. Dekkers (2001), The application of fuzzy C-means cluster analysis and non-linear mapping to a soil data set for the detection of polluted sites, *Phys. Chem. Earth.*, *26*, 885–891.
Hewitt, C. D., R. J. Stouffer, A. J. Broccoli, J. F. B. Mitchell, and P. J. Valdes (2003), The effect of ocean dynamics in a coupled GCM simulation of the Last Glacial Maximum, *Clim. Dyn.*, *20*, 203–218.
Hillaire-Marcel, C., A. de Vernal, G. Bilodeau, and G. Wu (1994), Isotope stratigraphy, sedimentation rates, deep circulation and carbonate events in the Labrador Sea during the last 200 ka, *Can. J. Earth Sci.*, *31*, 63–89.
Kassens, H. (1990), Verfestigte Sedimentlagen und seismische Reflektoren: Fruhdiagenese und Palaeo-ozeanographie in der Norwegischen See, *Ber. Sonderforsch. 313*, Christian-Albrechts-Univ., Kiel, Germany.
Keigwin, L. D. (2004), Radiocarbon and stable isotope constraints on Last Glacial Maximum and Younger Dryas ventilation in the western North Atlantic, *Paleoceanography*, *19*, PA4012, doi:10.1029/2004PA001029.
Kim, S. J., G. M. Flato, and G. J. Boer (2003), A coupled climate model simulation of the Last Glacial Maximum, part 2: Approach to equilibrium, *Clim. Dyn.*, *20*, 635–661.
Kissel, C. (2005), Magnetic signature of rapid climatic variations in glacial North Atlantic: A review, *C. R. Geosci.*, *337*, 908–918.
Kissel, C., C. Laj, B. Lehman, L. Labeyrie, and V. Bout-Roumazeilles (1997), Changes in the strength of the Iceland-Scotland Overflow Water in the last 200,000 years: Evidence from magnetic anisotropy analysis of core SU90-33, *Earth Planet. Sci. Lett.*, *152*, 25–36.
Kissel, C., C. Laj, L. Labeyrie, T. Dokken, A. Voelker, and D. Blamart (1999), Rapid climatic variations during marine isotopic stage 3: Magnetic analysis of sediments from Nordic Seas and North Atlantic, *Earth Planet. Sci. Lett.*, *171*, 489–502.
Knies, J. (1999), Late Quaternary paleoenvironment along the northern Barents and Kara seas continental margin: A multi parameter analysis, *Rep. Polar Res. 304*, Alfred Wegener Inst. for Polar and Mar. Res., Bremerhaven, Germany.
LeGrand, P., and C. Wunsch (1995), Constraints from paleotracer data on the North Atlantic circulation during the Last Glacial Maximum, *Paleoceanography*, *10*, 1011–1045.
Linthout, K., S. R. Troelstra, and A. Kuijpers (2000), Provenance of coarse ice-rafted detritus near the SE Greenland margin, *Geol. Mijnbouw*, *79*, 109–121.
Maher, B. A. (1988), Magnetic properties of some synthetic sub-micron magnetites, *Geophys. J.*, *94*, 83–96.
Maher, B. A. (1998), Magnetic properties of modern soils and Quaternary loessic paleosols: Paleoclimatic implications, *Palaeogeogr. Palaeoclimatol. Palaeoecol.*, *137*, 25–54.
Maher, B. A., and P. F. Dennis (2001), Evidence against dust-mediated control of glacial-interglacial changes in atmospheric CO_2, *Nature*, *411*, 176–180.
Maher, B. A., R. Thompson, and M. W. Hounslow (1999), Introduction, in *Quaternary Climates, Environments and Magnetism*, edited by B. A. Maher and R. Thompson, pp. 1–48, Cambridge Univ. Press, New York.
Marchal, O., R. François, T. F. Stocker, and F. Joos (2000), Ocean thermohaline circulation and sedimentary $^{231}Pa/^{230}Th$ ratio, *Paleoceanography*, *15*, 625–641.
McIntyre, A., N. G. Kipp, A. W. H. Be, T. Crowley, T. Kellogg, J. V. Gardner, W. Prell, and W. F. Ruddiman (1976), Glacial North Atlantic 18000 years ago: A CLIMAP reconstruction, in *Investigation of Late Quaternary Paleoceanography and Paleoclimatology*, edited by R. M. Cline and J. D. Hays, *Mem. Geol. Soc. Am.*, *145*, 43–76.
McManus, J. F., R. Francois, J. M. Gherardi, L. D. Keigwin, and S. Brown-Leger (2004), Collapse and rapid resumption of Atlantic meridional circulation linked to deglacial climate changes, *Nature*, *428*, 834–837.
Meland, M. Y., E. Jansem, and F. Elderfield (2005), Constraints on SST estimates for the northern North Atlantic/Nordic Seas during the LGM, *Quat. Sci. Rev.*, *24*, 835–852.
Michel, E., L. D. Labeyrie, J.-C. Duplessy, N. Gorfti, M. Labracherie, and J.-L. Turon (1995), Could deep Subantarctic convection feed the world deep basins during the Last Glacial Maximum?, *Paleoceanography*, *10*, 927–942.
Oppo, D. W., and R. G. Fairbanks (1987), Variability in the deep and intermediate water circulation of the Atlantic Ocean during the past 25,000 years: Northern Hemisphere modulation of the Southern Ocean, *Earth Planet. Sci. Lett.*, *86*, 1–15.
Pailler, D., and E. Bard (2002), High frequency palaeoceanographic changes during the past 140,000 yr recorded by the organic matter in sediments of the Iberian Margin, *Palaeogeogr. Palaeoclimatol. Palaeoecol.*, *181*, 431–452.
Peck, V. L., I. R. Hall, R. Zahn, H. Elderfield, F. Grousset, S. R. Hemming, and J. D. Scourse (2006), High resolution evidence for linkages between NW European ice sheet instability and Atlantic meridional overturning circulation, *Earth Planet. Sci. Lett.*, *243*, 476–481.
Peltier, W. R. (1994), Ice age paleotopography, *Science*, *265*, 195–201.
Pflaumann, U., et al. (2003), Glacial North Atlantic: Sea-surface conditions reconstructed by GLAMAP 2000, *Paleoceanography*, *18*(3), 1065, doi:10.1029/2002PA000774.
Prins, M. A., L. M. Bouwer, C. J. Beets, G. J. Troelstra, R. W. Kruk, A. Kuijpers, and P. Z. Vroon (2002), Ocean circulation and iceberg discharge in the glacial North Atlantic: Inferences from unmixing of sediment size distributions, *Geology*, *30*, 555–558.
Prospero, J. M., R. A. Glaccum, and R. T. Nees (1981), Atmospheric transport of soil dust from Africa to South America, *Nature*, *289*, 570–572.
Rahmstorf, S. (2002), Ocean circulation and climate during the past 120,000 years, *Nature*, *419*, 207–214.
Rasmussen, T. L., T. C. E. van Weering, and L. Labeyrie (1997), Climatic instability, ice sheets and ocean dynamics at high northern latitudes during the last glacial period (58–10 ka BP), *Quat. Sci. Rev.*, *16*, 71–80.
Revel, M., J. A. Sinko, F. E. Grousset, and H. de Hass (1996), Sr and Nd isotopes as tracers of North Atlantic lithic particles: Paleoclimate implications, *Paleoceanography*, *11*, 95–113.
Richter, T. O., S. Lassen, T. C. E. van Weering, and H. de Haas (2001), Magnetic susceptibility patterns and provenance of ice-rafted material at Feni Drift, Rockall Trough: Implications for the history of the British-Irish ice sheet, *Mar. Geol.*, *173*, 37–54.
Robinson, S. G. (1986), The late Pleistocene palaeoclimatic record of North Atlantic deep-sea sediments revealed by mineral magnetic measurements, *Phys. Earth Planet. Inter.*, *42*, 22–47.
Robinson, S. G., M. A. Maslin, and I. N. McCave (1995), Magnetic susceptibility variations in upper Pleistocene deep-sea sediments of the NE Atlantic: Implications for ice rafting and paleocirculation at the Last Glacial Maximum, *Paleoceanography*, *10*, 221–250.
Robinson, L. F., J. F. Adkins, L. D. Keigwin, J. Southon, D. P. Fernandez, S.-L. Wang, and D. S. Scheirer (2005), Radiocarbon variability in the western North Atlantic during the last deglaciation, *Science*, *310*, 1469–1473.
Ruddiman, W. F. (1977), Late Quaternary deposition of ice-rafted sand in the subpolar North Atlantic (lat 40 to 65N), *Geol. Soc. Am. Bull.*, *88*, 1813–1827.
Sarnthein, M., K. Winn, S. J. A. Jung, J.-C. Duplessey, L. Labeyrie, H. Erienkeuser, and G. Ganssen (1994), Changes in east Atlantic deepwater circulation over the last 30,000 years: Eight time slice reconstructions, *Paleoceanography*, *9*, 209–267.
Sarnthein, M., et al. (1995), Variations in Atlantic surface ocean paleoceanography, 50–80N: A time-slice record of the past 30,000 years, *Paleoceanography*, *10*, 1063–1094.
Schäfer-Neth, C., and A. Paul (2000), Circulation of the glacial Atlantic: A synthesis of global and regional modelling, in *The Northern North Atlantic: A Changing Environment*, edited by P. Schäfer et al., pp. 441–462, Springer, New York.
Seidov, D., and B. J. Haupt (1997), Simulated ocean circulation and sediment transport in the North Atlantic during the Last Glacial Maximum and today, *Paleoceanography*, *12*, 281–305.
Seidov, D., M. Sarnthein, K. Stattegger, R. Prien, and M. Weinelt (1996), North Atlantic ocean circulation during the Last Glacial Maximum

and subsequent meltwater events: A numerical model, *J. Geophys. Res.*, *101*, 16,305–16,332.
Seidov, D., B. J. Haupt, and M. Maslin (Eds.) (2001), *The Oceans and Rapid Climate Change: Past, Present and Future*, *Geophys. Monogr. Ser.*, vol. 126, edited by D. Seidov, B. J. Haupt, and M. Maslin 293 pp., AGU, Washington, D. C.
Shin, S. I., Z. Liu, B. Otto-Bliesner, E. C. Brady, J. E. Kutzbach, and S. P. Harrison (2003), A simulation of the Last Glacial Maximum climate using the NCAR-CCSM, *Clim. Dyn.*, *20*, 127–151.
Smith, S. D., and E. G. Banke (1983), The influence of winds, currents and towing force on the drift of icebergs, *Cold Reg. Sci. Technol.*, *6*, 241–245.
Smythe, F. W., W. F. Ruddiman, and D. N. Lumsden (1985), Ice-rafted evidence of long-term North Atlantic circulation, *Mar. Geol.*, *64*, 131–141.
Stein, R., S. Nam, H. Grobe, and H.-W. Hubberton (1995), Late Quaternary history and short-term ice-rafted debris fluctuations along the East Greenland continental margin, in *Late Quaternary Paleoceanography of the North Atlantic Margins*, edited by J. Andrews et al., *Geol. Soc. Spec. Publ.*, *111*, 135–151.
St. John, K., B. P. Flower, and L. Krissek (2004), Evolution of iceberg melting, biological productivity, and the record of Icelandic volcanism in the Irminger basin since 630 ka, *Mar. Geol.*, *212*, 133–152.
Stoner, J. S., J. E. T. Channell, and C. Hillaire-Marcel (1996), The magnetic signature of rapidly deposited detrital layers from the deep Labrador Sea: Relationship to North Atlantic Heinrich layers, *Paleoceanography*, *11*, 309–325.
Thompson, R., and F. Oldfield (1986), *Environmental Magnetism*, 227 pp, Allen and Unwin, St. Leonards, N. S. W., Australia.
Vogt, C. (1997), Regional and temporal variations of mineral assemblages in Arctic Ocean sediments as climate indicator during glacial/interglacial changes, *Rep. Polar Res. 251*, 309 pp., Alfred Wegener Inst. for Polar and Mar. Res. Bremerhaven, Germany.
Vriend, S. P., P. F. M. van Gaans, J. Middelburg, and A. de Nus (1988), The application of fuzzy C-means cluster analysis and non-linear mapping to geochemical datasets: Examples from Portugal, *Appl. Geochem.*, *3*, 213–224.
Wadley, M. R., and G. R. Bigg (2002), Impact of flow through the Canadian Archipelago and Bering Strait on the North Atlantic and Arctic circulation: An ocean modelling study, *Q. J. R. Meteorol. Soc.*, *128*, 2187–2203.
Wadley, M. R., G. R. Bigg, E. J. Rohling, and A. J. Payne (2002), On modelling present-day and Last Glacial Maximum oceanic δ^{18}O distribution, *Global Planet. Change*, *32*, 89–109.
Watkins, S. J. (2003), Geological ground-truthing of modelled iceberg trajectories in the North Atlantic: Present day and Last Glacial Maximum, Ph. D. thesis, Sch. of Environ. Sci., Univ. of East Anglia, Norwich, U. K.
Watkins, S. J., and B. A. Maher (2003), Magnetic characterisation of present-day deep-sea sediments and sources in the North Atlantic, *Earth Planet. Sci. Lett.*, *214*, 379–394.
Yu, E.-F., R. Francois, and M. P. Bacon (1996), Similar rates of modern and last-glacial ocean thermohaline circulation inferred from radiochemical data, *Nature*, *379*, 689–694.

G. R. Bigg, Department of Geography, University of Sheffield, Winter Street, Sheffield S10 2TN, UK.

B. A. Maher and S. J. Watkins, Centre for Environmental Magnetism and Palaeomagnetism, Lancaster Environment Centre, Geography Department, Lancaster University, Lancaster LA1 4YB, UK. (b.maher@lancaster.ac.uk; sarah.watkins@lancaster.ac.uk)